



OPEN ACCESS

ORIGINAL RESEARCH

# FLCN-regulated miRNAs suppressed reparative response in cells and pulmonary lesions of Birt-Hogg-Dubé syndrome

Haiyan Min,<sup>1,2</sup> Dehua Ma,<sup>3</sup> Wei Zou,<sup>4</sup> Yongzheng Wu,<sup>1,2</sup> Yibing Ding,<sup>1,2</sup> Chengchu Zhu,<sup>3</sup> Anqi Lin,<sup>1,2</sup> Shiyu Song,<sup>1,2</sup> Qiao Liang,<sup>1,2</sup> Baofu Chen,<sup>3</sup> Bin Zhang,<sup>1</sup> Yueming Wan,<sup>5</sup> Minhua Ye,<sup>3</sup> Yanqing Pan,<sup>4</sup> Yanting Wen,<sup>1,2</sup> Long Yi,<sup>1,2</sup> Qian Gao

► Additional material is published online only. To view please visit the journal online (<http://dx.doi.org/10.1136/thoraxjnl-2019-213225>).

For numbered affiliations see end of article.

## Correspondence to

Professor Qian Gao, Jiangsu Key Laboratory for Molecular Medicine, Nanjing University Medical School, Nanjing 210093, China; [qian\\_gao@nju.edu.cn](mailto:qian_gao@nju.edu.cn)

HM and DM contributed equally.

Received 13 February 2019  
Revised 21 December 2019  
Accepted 28 January 2020  
Published Online First  
17 March 2020



► <http://dx.doi.org/10.1136/thoraxjnl-2019-214112>  
► <http://dx.doi.org/10.1136/thoraxjnl-2020-214861>



© Author(s) (or their employer(s)) 2020. Re-use permitted under CC BY-NC. No commercial re-use. See rights and permissions. Published by BMJ.

**To cite:** Min H, Ma D, Zou W, et al. *Thorax* 2020;**75**:476–485.

## ABSTRACT

**Background** Birt-Hogg-Dubé Syndrome (BHDS) characterised by skin fibrofolliculomas, kidney tumour and pulmonary cysts/pneumothorax is caused by folliculin (FLCN) germline mutations. The pathology of both neoplasia and focused tissue loss of BHDS strongly features tissue-specific behaviour of the gene. Isolated cysts/pneumothorax is the most frequent atypical presentation of BHDS and often misdiagnosed as primary spontaneous pneumothorax (PSP). Differential diagnosis of BHDS with isolated pulmonary presentation (PSP-BHD) from PSP is essential in lifelong surveillance for developing renal cell carcinoma.

**Methods** The expression profiles of microRNAs (miRNAs) in cystic lesions of PSP-BHD and PSP were determined via microarray. The selected upregulated miRNAs were further confirmed in the plasma of an expanded cohort of PSP-BHD patients by reverse transcription quantitative PCR (RT-qPCR). Their diagnostic accuracy was evaluated. Moreover, the cellular functions and targeted signalling pathways of FLCN-regulated miRNAs were assessed in various cell lines and in the lesion tissue contexts.

**Results** Cystic lesions of PSP-BHD and PSP showed different miRNAs profiles with a significant upregulation of miR-424–5p and let-7d-5p in PSP-BHD. The combination of the two effectively predicted BHDS patients. In vitro studies revealed a suppressive effect of FLCN on miR-424–5p and let-7d-5p expressions specifically in lung epithelial cells. The ectopic miRNAs triggered epithelial apoptosis and epithelial transition of mesenchymal cells and suppressed the reparative responses in cells and tissues with FLCN deficiency.

**Conclusion** The upregulation of miR-424–5p and let-7d-5p by FLCN deficiency occurred in epithelial cells and marked the PSP-BHD condition, which contributed to a focused degenerative pathology in the lung of PSP-BHD patients.

## INTRODUCTION

Birt-Hogg-Dubé syndrome (BHDS) characterised by skin fibrofolliculomas, pulmonary cysts/pneumothorax and increased risk of kidney cancers is an autosomal dominant disease caused by germline mutations of folliculin (FLCN) gene.<sup>1</sup> It is often misdiagnosed as primary spontaneous pneumothorax (PSP) in particular in the cases with only isolated lung cysts/pneumothorax presentation

## Key messages

### What is the key question?

► Varied pathological presentations of Birt-Hogg-Dubé syndrome (BHDS) indicate tissue-specific function of the causal gene folliculin (FLCN), which was widely studied mechanistically in the kidney tumours but poorly elucidated in lung cysts/pneumothorax presentation.

### What is the bottom line?

► FLCN negatively regulated miR-424–5p and let-7d-5p expressions specifically in lung epithelial cells, and thus caused a significant increase of the two in both lung tissue and circulation in FLCN mutant BHD patients, which resulted in an increased apoptosis of lung epithelial cells and mesenchymal–epithelial transition of fibroblasts, qualified them as diagnostic markers for disease screen.

### Why read on?

► The mechanism revealed in this study is specific to the lung, and implies that the miRNAs regulated by FLCN suppressed cell reparative response in the lung tissue and contributed to a focused degenerative pathology in BHDS' lung.

(PSP-BHD).<sup>2–4</sup> An early and definitive recognition of PSP-BHD that is broadly underdiagnosed from PSP is necessary for a lifelong surveillance due to an increased risk for developing kidney tumours.<sup>5–7</sup>

Genetic analysis of FLCN gene consists of sequence analysis and exonic deletion and amplification detection.<sup>8</sup> With this approach, we have previously found in a cohort study that about 10% of hospitalised PSP patients who were not considered to initiate a genetic examination of FLCN gene were actually BHDS sufferers.<sup>2</sup> Thus, a screen of PSP population with a technically simpler and more affordable tool before a genetic analysis of BHDS is desirable.

microRNAs (miRNAs) have been served as the signature for various diseases including genetic disorders.<sup>9–11</sup> In fact, a robust miRNA signature often indicates a mechanistic role of the targets of miRNAs in the disease development, and thus composes of an effective tool to dissect disease



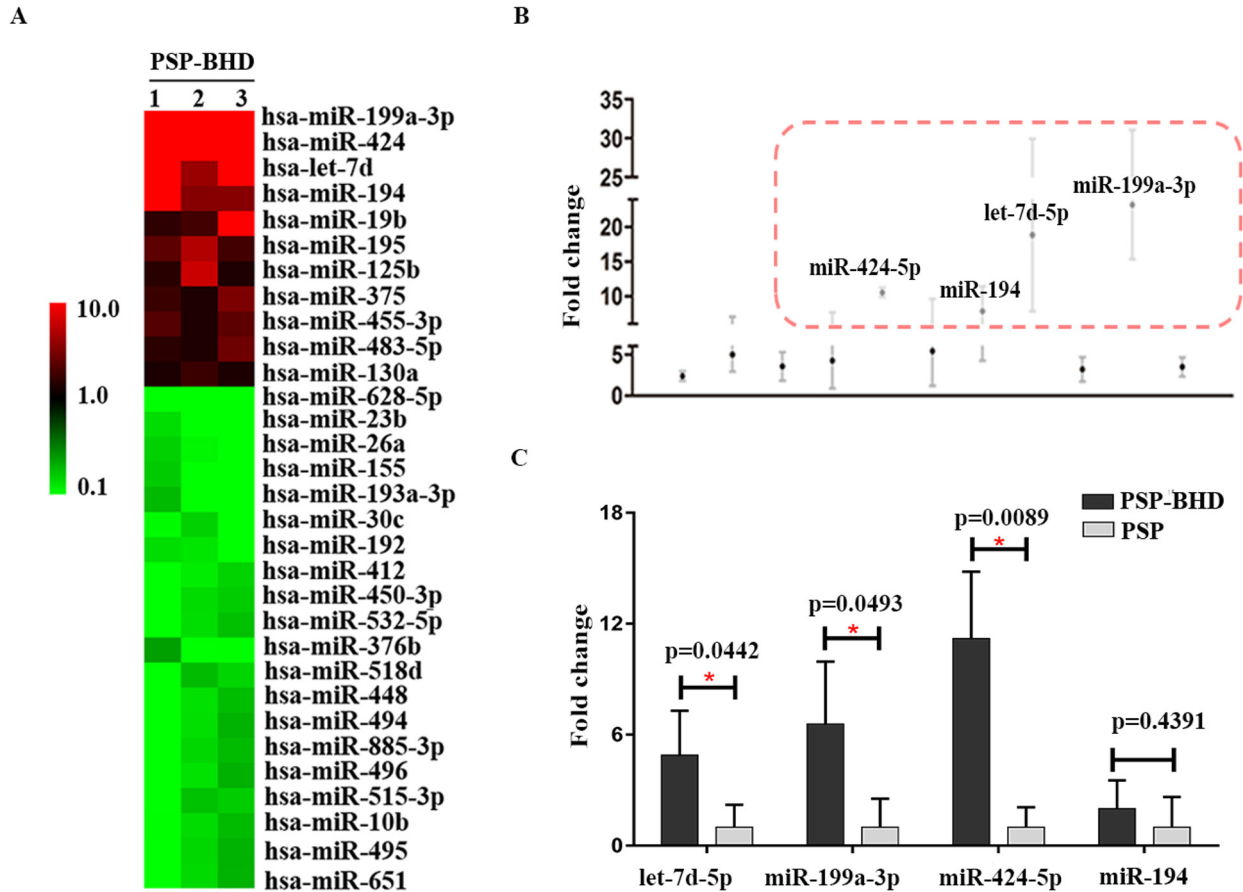


**Figure 1** miRNA signature uncovered in BHD cystic lesions. (A) Represented miRNAs dysregulated in cystic lesions of PSP-BHD (n=3) compared to that of PSP (n=3) patients. Mutations of FLCN gene are p.(P63TfsX69), p.(S316YfsX73) and p.(Arg527GlnfsX75). (B) Four miRNAs were found fivefold or more increase in PSP-BHD in microarray analysis. (C) Increases of miR-424-5p, let-7d-5p and miR-199a-3p were confirmed in cystic lesions of PSP-BHD (n=14) compared to that of PSP patients (n=14). The mutation information of PSP-BHD patients was in online supplementary table 1. The columns represent mean and the bars indicate SD. BHD, Birt-Hogg-Dubé syndrome; FLCN, folliculin; miRNA, microRNA; PSP, primary spontaneous pneumothorax. \* Represents statistical significance.

mechanism.<sup>12 13</sup> However, in FLCN study, the involvement of miRNAs in the pathogenesis of pulmonary cysts in BHDS is under studied. Nevertheless, the characteristic histology of the lung lesions of BHDS exhibits no obvious inflammation and reparative response,<sup>14</sup> implicating a suppressive nature of FLCN deficiency on the mesenchyme that is essential in damage-related tissue repairing. On the other hand, in a mouse model of FLCN-null in lung type II alveolar epithelial cells, an increased epithelial apoptosis is detected.<sup>15</sup> These observations indicate an involvement of epithelial damage and mesenchymal suppression, however, no cystic lesions are ever induced experimentally. Thus, the molecular mechanism that may explain lesion pathology of PSP-BHD deserves a systematic exploration.

Herein, we sought to identify miRNAs differentially expressed in PSP-BHD and PSP patients for a diagnostic application and for elucidating the molecular mechanisms of these miRNAs in the pathogenesis of the disease.

## METHODS

### Population

PSP patients admitted according to the guidelines of the British Thoracic Society<sup>16</sup> and normal controls (NCs) were enrolled to Department of Cardiothoracic Surgery of Taizhou Hospital of Zhejiang Province and Nanjing Chest Hospital between 2006 and 2015.

### Cell lines

Human bronchial epithelial cells (BEAS-2B), human lung epithelial A549 cells, human keratinocyte cells (HaCaT), human embryonic lung fibroblasts (HELFI) and human embryonic kidney cells (HEK293) were purchased from China Center for Type Culture Collection.

### miRNAs assay, quantitative PCR analysis and Western blot

For miRNAs screen, Universal Probe Library assays (Roche) were used. For miRNA/mRNA or protein detection, RT-qPCR or western blot (WB) was used, respectively.

### Apoptosis detection

Apoptosis in cultured cells was analysed by AnnexinV-FITC and propidium iodide staining using a caliber flow cytometer (BD Biosciences). Apoptosis in the lung tissues was analysed with TdT-mediated dUTP Nick-End Labeling (TUNEL) assays using in situ Cell Death Detection Fluorescein Kit (Roche).

### Luciferase reporter construction and assay

The target sequences of Smad7 and Frizzled 4 (FZD4) 3'-Untranslated Region (3' UTR) were amplified and subcloned (Realgene) into a dual-luciferase reporter vector (Promega), respectively. The luciferase reporter assays were performed in HEK293 cells.

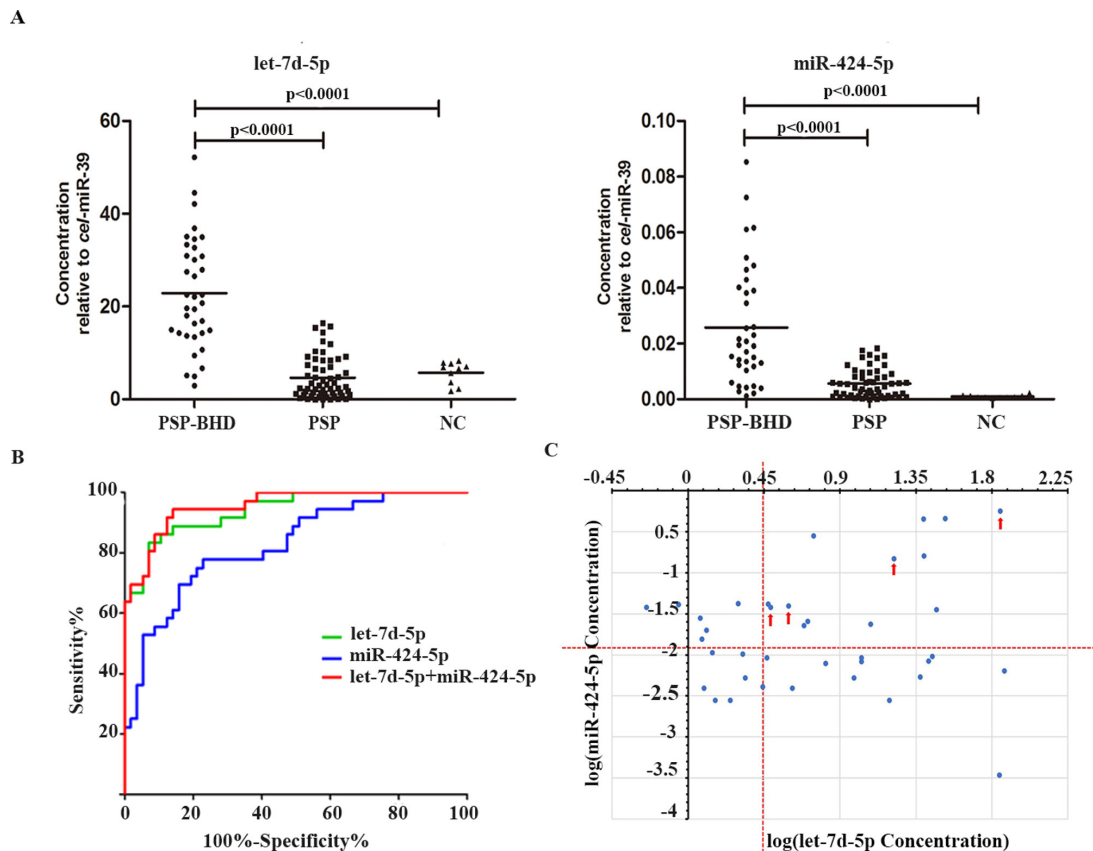


**Figure 2** Plasma miR-424-5p and let-7d-5p differentially diagnosed PSP-BHD from PSP. (A) The relative concentration of miR-424-5p and let-7d-5p to cel-miR-39 in plasma of PSP-BHD patients (n=36), PSP patients (n=57) and normal controls (NCs) (n=15). NC represents normal controls. The dashes represent the mean values. A stepwise linear regression by SPSS V.17.0 was used to conclude that FLAN mutation was a major contributor to the expressions of miR-424-5p and let-7d-5p (online supplementary table 3). (B) ROC curves of plasma detections as signal or combined biomarkers. (C) The relative concentrations of miR-424-5p and let-7d-5p to cel-miR-39 in plasma of PSP population (n=38) of the prospective study. The red dotted lines are the cut-off values of miR-424-5p and let-7d-5p. The red arrows indicated BHD patients confirmed by genetic analysis. BHD, Birt-Hogg-Dubé syndrome; FLCN, folliculin; PSP, primary spontaneous pneumothorax; ROC, receiver operating characteristic.

### Immunohistochemistry and H&E staining

Tissues were fixed in 4% paraformaldehyde and embedded in paraffin. Tissue sections (7  $\mu$ m) were prepared for immunohistochemistry of Smad7, FZD4, Vimentin,  $\alpha$ -smooth muscle actin ( $\alpha$ -SMA), tight junction protein 1 (TJP1) and Snail, and for H&E staining.

### Data analysis and statistics

Receiver operator characteristic (ROC) curves were generated by plotting Sensitivity% versus (100%-specificity%) and the areas under the curves (AUCs) were calculated. Logistic regression analysis was used for the evaluation of the accuracy of combined

**Table 1** Diagnostic accuracies of measurements of single markers for predicting PSP-BHD at predefined specificities and sensitivities

	AUC (95% CI)	Sensitivity at 90%: specificity, %	Sensitivity at 90%: specificity, %:
let-7d-5p	0.93 (0.88 to 0.99)	73.1	82.1
miR-424-5p	0.87 (0.79 to 0.95)	58	64.3
let-7d-5p+miR-424-5p	0.96 (0.92 to 1.00)	90.4	92.9

AUC, area under the curve; BHD, Birt-Hogg-Dubé syndrome; PSP, primary spontaneous pneumothorax.

miRNA markers. For WB and wound-healing experiments data quantified by ImageJ, and for qPCR data of miRNA/mRNA levels, Student's t-test was used. For plasma miRNA levels, Tukey's test followed by Duncan's multiple range test was used. All statistical analyses were performed with either SPSS V.17.0 or GraphPad Prism V.5.0 Software (quantifying uncertainty of 95% CIs and statistical significance of  $p < 0.05$ ) and all p values of comparisons were detailed in online supplementary files.

The details of the methods were provided in online supplementary methods.

## RESULTS

### miRNA signature uncovered in BHD cystic lesions

We initially compared the expression profiles of miRNAs in cystic lesions of PSP-BHD patients to that of PSP patients (n=3, respectively) via a commercialised microarray (Roche). Totally, 11 upregulated and 52 downregulated miRNAs were uncovered in the cystic tissues of PSP-BHD patients when compared with that of PSPs (figure 1A and see online supplementary table 4). Wntless/integrated (WNT), transforming growth factor- $\beta$  (TGF- $\beta$ ), epidermal growth factor receptor (ErbB), mitogen-activated protein kinase (MAPK), phosphatidylinositol 3'-kinase (PI3K)-Akt (PI3K-Akt) and mammalian target of rapamycin (mTOR) signalling pathways were targeted by these miRNAs on DIANA-miRPath V.2.0 prediction<sup>17 18</sup> (see online supplementary

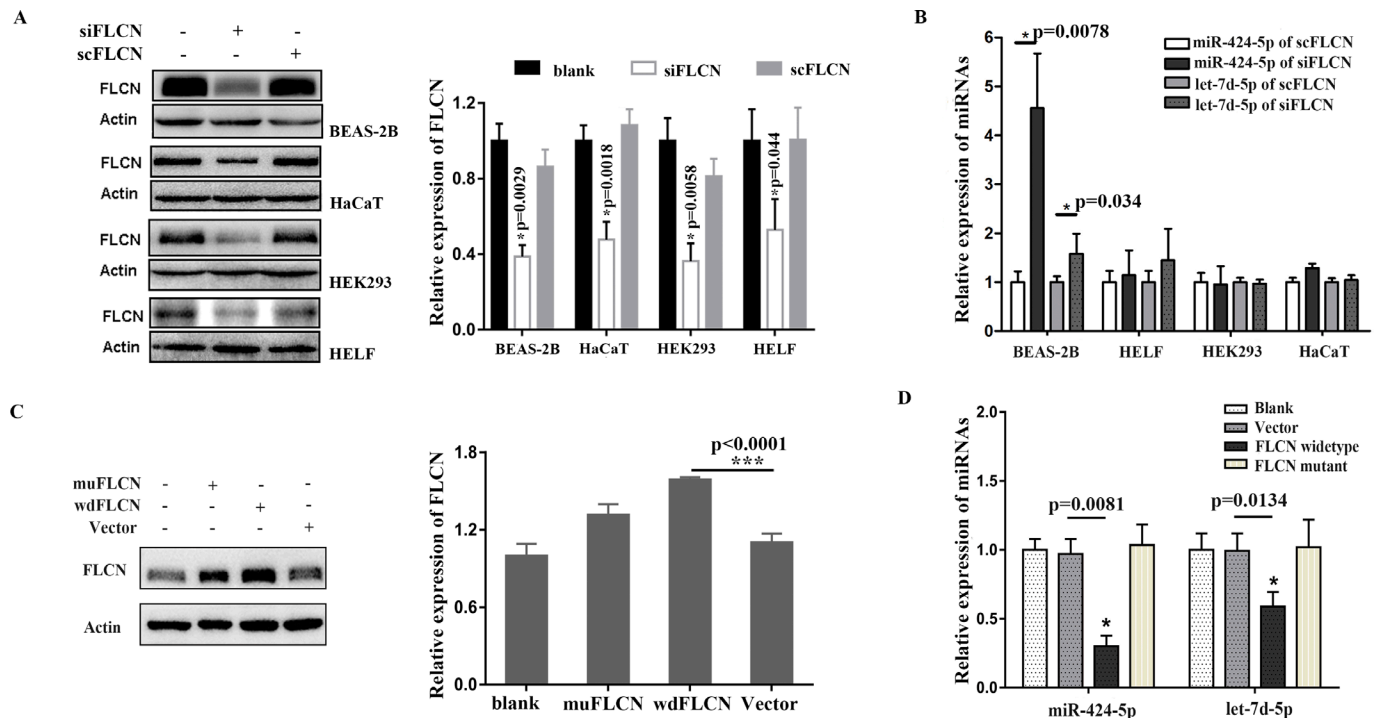


**Figure 3** FLCN suppressed miR-424-5p and let-7d-5p expressions in lung epithelial cells. (A) Endogenous FLCN was knocked down by siRNA in different cell lines and was statistically calculated with four times experiments. (B) The expression of miR-424-5p and let-7d-5p in different cells with FLCN knockdown. siFLCN means a siRNA sequence of FLCN, scFLCN means a scramble sequence of FLCN. (C) Protein expression of FLCN in A549 cells with wildtype-FLCN-expressed plasmids (wdFLCN), mutant-FLCN expressed plasmids (muFLCN) and blank vectors and was statistically calculated with four times experiments. FLCN mutant was p.(Arg527Glnfs\*75). (D) The expression of miR-424-5p and let-7d-5p in A549 cells with wdFLCN, muFLCN and vectors. The columns represent mean and the bars indicate SD. FLCN, Folliculin.

table 5). Since downregulated miRNA may not be ideal as biomarker for diagnosis, four upregulated miRNAs with fivefold or more increase in PSP-BHD patients, including miR-424-5p, let-7d-5p, miR-199a-3p and miR-194, were arbitrary chosen for subsequent studies (figure 1B). In an expanded collection of PSP-BHD and an equal number of PSP lesion samples (n=14), the expressions of miR-424-5p, miR-199a-3p and let-7d-5p were confirmed to be increased in PSP-BHD with 10-fold, 6.6-fold and 4.9-fold changes, respectively, when compared with those of PSP (figure 1C). Thus, PSP-BHD cystic lesion exhibited specific miRNA signature.

### Plasma miR-424-5p and let-7d-5p differentially diagnosed PSP-BHD from PSP

To determine whether the upregulated miRNAs in the cystic lesion may appropriately serve as biomarkers for differential diagnosis between PSP-BHD and PSP, the relative levels of the three miRNAs were determined in the plasma of 36 PSP-BHD and 57 PSP patients, as well as 15 NC. As expected, miR-424-5p and let-7d-5p were significantly higher in PSP-BHD patients compared with those of PSP and NC individuals (figure 2A). However, the relative concentration of miR-199a-3p in PSP-BHD plasma was equivalent to that of NC, but obviously reduced in PSP patients (see online supplementary figure S1), thus, resulted in the selection of miR-199a-3p in the initial screen.

Next, the ROC curves were constructed by comparing plasma measurements of the identified miRNAs in PSP-BHD and PSP groups. The AUCs were calculated. The single AUC of miR-424-5p or let-7d-5p was 0.87 or 0.93, respectively, and the AUC of the two combined was improved to 0.96 (figure 2C and table 1). The sensitivity at the fixed specificity of 90% of

the combination were also improved and vice versa (table 1). The cut-off values of miR-424-5p and let-7d-5p calculated on Yuden index were 0.0116 and 2.839 that resulted in 100% sensitivity and 62% specificity. Using these values, we screened a cohort of 38 genetically undefined PSP patients with blind of any additional clinical information. A total 13 candidates for BHDs were suggested and 4 of them (31%) were eventually confirmed to be FLCN-mutation carriers by genetic examinations. None of the rest 25 PSP patients was FLCN-mutation carrier (figure 2C). Thus, the miRNA screen cut down about 2/3 (65.8%) genetic analysis of FLCN that is largely unavailable in local clinics.

### FLCN negatively regulated miR-424-5p and let-7d-5p in lung epithelial cells

Subsequently, a set of human cell lines with different origins including the lung epithelial cell BEAS-2B, embryonic lung fibroblast HELF, skin epithelial cell HaCaT and embryonic kidney cell HEK293 were prepared for FLCN knockdown studies (figure 3A). On FLCN disruption, the expressions of miR-424-5p and let-7d-5p were significantly increased only in BEAS-2B cells (figure 3B), suggesting a cell-specific regulation of the two by FLCN. In consistent, in a lung epithelial cell line A549 with low endogenous FLCN (figure 3C), the ectopic expression of a wild type FLCN gene resulted in a significant downregulation of miR-424-5p and let-7d-5p. In contrast, a disease-causing mutation (p.(Arg527Glnfs\*75))<sup>19</sup> deprived this suppressive function of FLCN (figure 3D). Thus, FLCN specifically and negatively regulated miR-424-5p and let-7d-5p in lung epithelial cells.

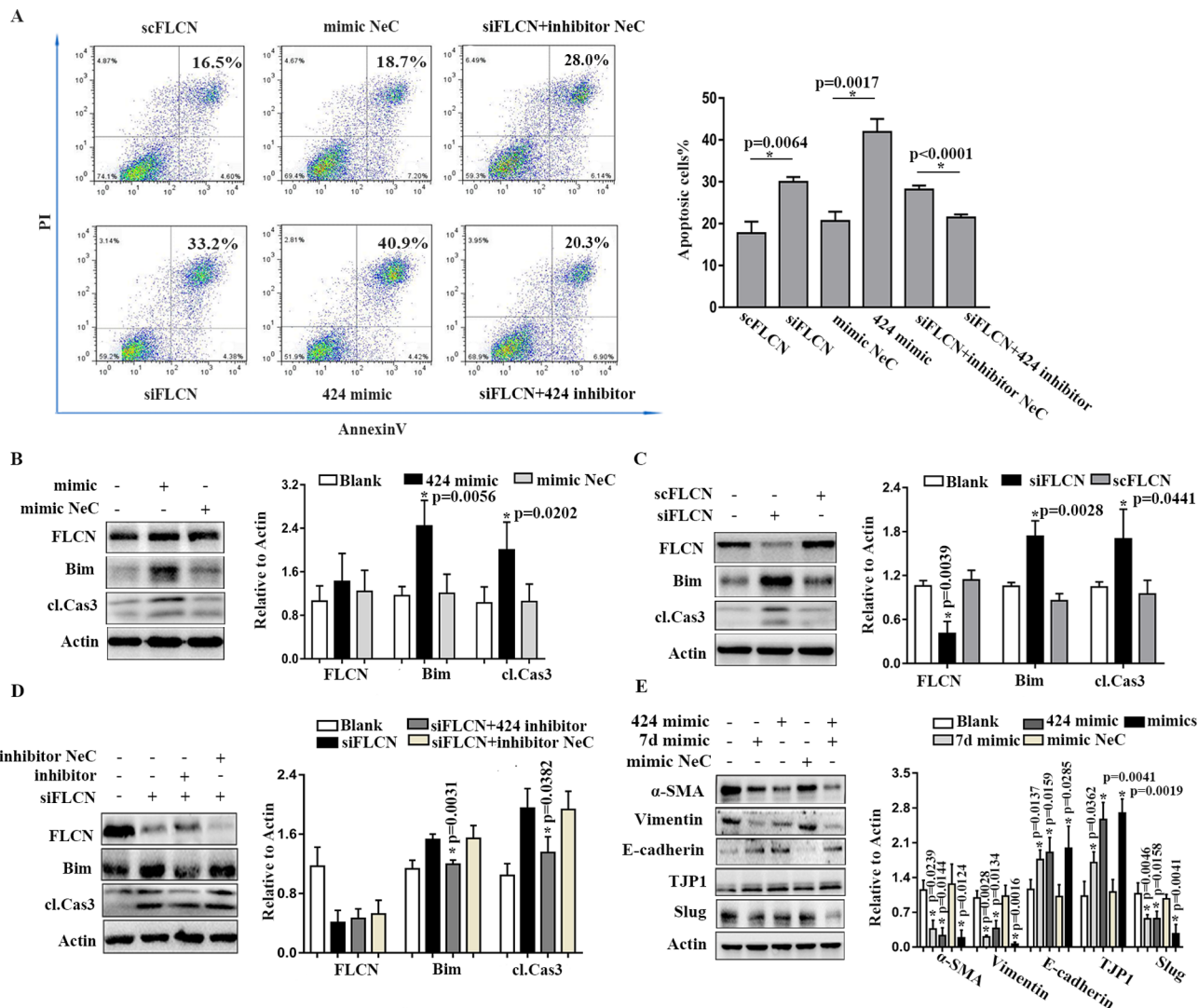


**Figure 4** FLCN-regulated miRNAs exhibited cell-specific functions. (A) Apoptosis of BEAS-2B cells was increased with FLCN interference or miR-424-5p mimic, respectively, and miR-424-5p inhibitor blocked the apoptosis of BEAS-2B cells induced by FLCN interference by FACS analysis with statistical calculation. (B, C) Bim and Cleaved Caspase3 (cl.Cas3) were upregulated with miR-424-5p mimic (B) or FLCN interference (C) with statistical calculation. P values were calculated by comparing with mimic NeC (B) or scFLCN (C). (D) The upregulation of Bim and cl.Cas3 induced by FLCN knockdown were blocked by miR-424-5p inhibitor in BEAS2B cells with statistical calculation. P values were calculated by comparing with inhibitor NeC. (E) Proteins of vimentin,  $\alpha$ -SMA and Slug were reduced significantly while TJP1 and E-Cadherin were increased in HELF cells with miR-424-5p and/or let-7d-5p mimics with statistical calculation. 424 represents miR-424-5p and 7d represents let-7d-5p. The columns of B–E represent mean of the relative expression and the bars indicate SD of the triplicate experiments. FLCN, folliculin; scFLCN, sequence of FLCN.

### FLCN-regulated miRNAs exhibited cell-specific functions

Next, we studied the functions of FLCN-regulated miRNAs in cells with different origins by introducing miR-424-5p and/or let-7d-5p mimics. Only miR-424-5p mimics in BEAS-2B cells induced apoptosis (figure 4A) with increased expressions of Bim and cleaved Caspase3 (cl.Cas3) (figure 4B). Consistently, FLCN knockdown also induced apoptosis in BEAS-2B, but not HaCaT, HELF or HEK293 cells, along with increased Bim and cl.Cas3 (figure 4A,C and see online supplementary figure S2). And, an inhibitor of miR-424-5p suppressed this effect of FLCN knockdown (figure 4A,D).

In lung fibroblast HELF, the introduction of miR-424-5p/let-7d-5p mimics potentially induced a mesenchymal–epithelial transition (MET) revealed by significant reduction of fibroblastic marker vimentin,  $\alpha$ -SMA and Slug, and increase of epithelial indicator TJP1 and E-Cadherin both at mRNA and protein levels (figure 4E and see online supplementary figure S3). No

obvious changes of these indicators were observed in HELF cells with FLCN knockdown (see online supplementary figure S2), suggesting that the introduction of miR-424-5p/let-7d-5p was necessary and sufficient for the induction of MET in HELF cells. We did not observe any of MET response in HaCaT or HEK293 cells by miR-424-5p/let-7d-5p (data not shown). Importantly, miR-424-5p/let-7d-5p mimics induced specific cell responses, apoptosis or MET, in FLCN knockdown BEAS-2B or HELF cells, respectively, at an equal potency as in non-FLCN knockdown BEAS-2B or HELF cells (see online supplementary figure S4).

### Cell-specific function of the miRNAs targeted TGF- $\beta$ or WNT pathway

To elucidate the signalling mechanisms underlying the functions of miR-424-5p and let-7d-5p, we analysed the targets of the two

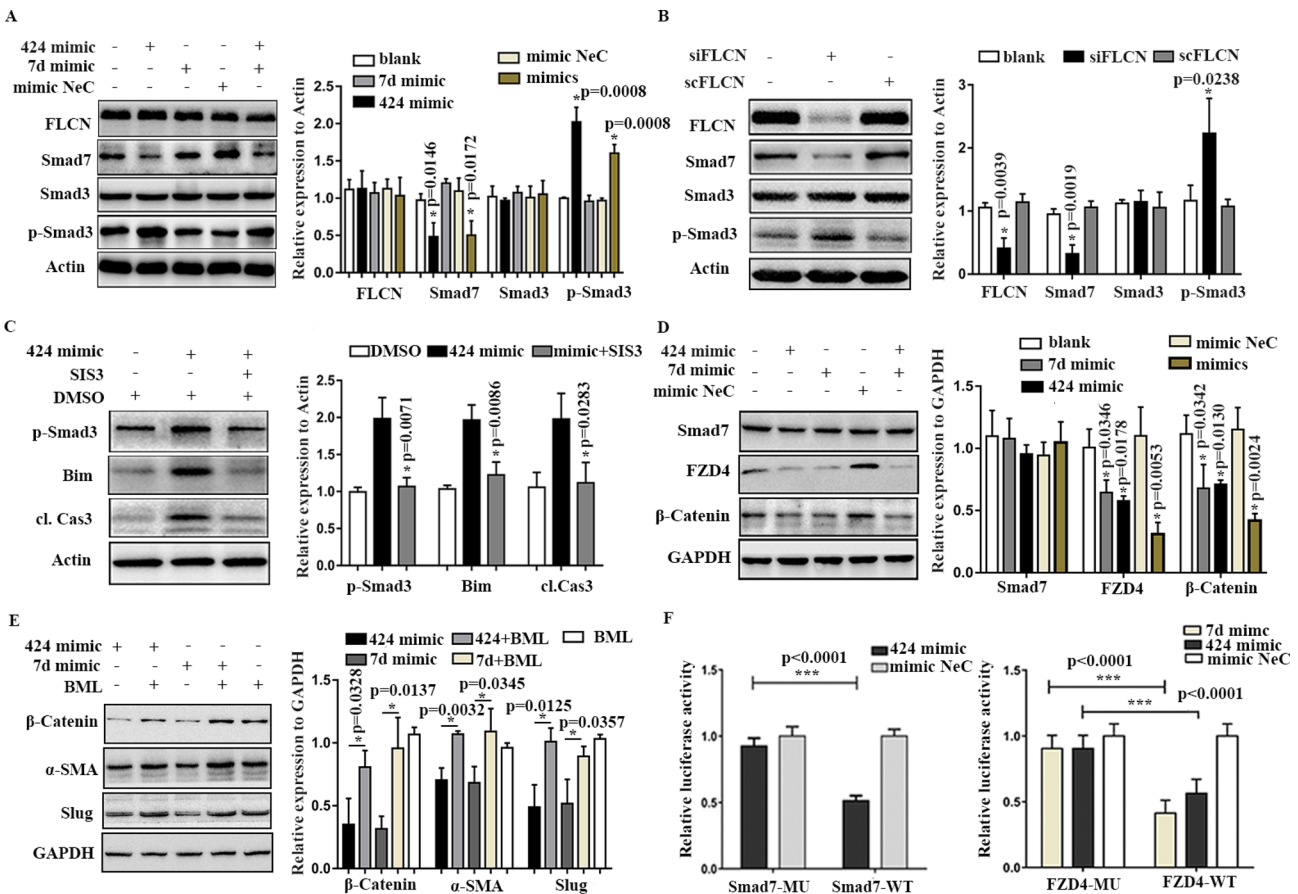


**Figure 5** Smad7 was targeted by miR-424-5p and FZD4 was targeted by both miR-424-5p and let-7d-5p. (A, B) Smad7 was suppressed and p-Smad3 was activated in BEAS-2B cells with miR-424-5p mimic (A) or FLCN knockdown (B) and was statistically analysed. (C) Inhibition of p-Smad3 by SIS3 suppressed the upregulation of Bim and cl.Cas3 with miR-424-5p mimic and was statistically analysed. (D) FZD4 and  $\beta$ catenin were downregulated with miR-424-5p or/and let-7d-5p mimics and was statistically analysed. (E) Activation of  $\beta$ -Catenin by BML restored the suppression of  $\alpha$ -SMA and Slug expression with miR-424-5p or let-7d-5p mimic and was statistically analysed. (F) The relative luciferase activity of Smad7 wildtype vectors was suppressed by miR-424-5p mimic and the relative luciferase activity of FZD4 wildtype vectors was suppressed by both miR-424-5p and let-7d-5p mimics with statistical significance. 424 represents miR-424-5p and 7d represents let-7d-5p. The columns in the figure represent mean of the relative expression and the bars indicate SD with triplicate experiments. cl.Cas3, cleaved Caspase3; FLCN, folliculin; scFLCN, scramble sequence of FLCN; siFLCN, sequence of FLCN.

through DIANA-miRPath V.2.0. Interestingly, three pathways (WNT, TGF- $\beta$  and mTOR pathways) were prominent in the prediction, which intersected the initial results uncovered in the microarray analysis (see online supplementary tables 5 and 6). Six candidates (see online supplementary table 6) in these pathways with higher affinity scores were chosen for further analysis. In BEAS-2B cells, only Smad7, a TGF- $\beta$  signalling component, was significantly suppressed by miR-424-5p mimics or FLCN knockdown, and the phosphorylation of its downstream Smad3 (p-Smad3) was largely increased (figure 5A,B). miR-424-5p in FLCN disrupted BEAS-2B cells showed similar results (see online supplementary figure S4). Importantly, a p-Smad3 inhibitor SIS3<sup>20</sup> blocked Bim and Caspase 3 activation induced by miR-424-5p (figure 5C), indicating that miR-424-5p targeted TGF- $\beta$  signalling is functionally crucial and cellular specific. Finally, the mimics of let-7d-5p showed no detectable effect of any on BEAS-2B cells.

In HELF cells both miR-424-5p and let-7d-5p mimics suppressed WNT signalling receptor FZD4. Accordingly, its downstream component  $\beta$ -Catenin was down-regulated (figure 5D). Whereas, an activator of  $\beta$ -Catenin<sup>21</sup> reversed the effect of both miR-424-5p and let-7d-5p mimics on induction

of MET in HELF cells (figure 5E). Noted of, FLCN knockdown alone in HELF cells did not show WNT signalling disruption (see online supplementary figure S2), yet both miR-424-5p and let-7d-5p mimics did, and importantly, both mimics worked in the condition of FLCN knockdown (see online supplementary figure S4). Together, miR-424-5p, as well as let-7d-5p mimics delivered different functions on the origin of cells by targeting either TGF- $\beta$  or WNT pathway. No change of mTOR signalling was detected in BEAS-2B or HELF cells (data not shown) on the introduction of miR-424-5p and let-7d-5p mimics.

Finally, the sequence specificity that targeted miR-424-5p to Smad7 3'UTR at the predicted position 55, and miR-424-5p/let-7d-5p to FZD4 3'UTR at the position 712 and 5028 were confirmed by relative luciferase activity assay (figure 5F) using the reporter constructs that cloned the corresponding miRNAs' target sequences (see online supplementary figure S6) in human embryonic kidney cell HEK293, a cell system commonly used for testing miRNA sequence specificity and function. Thus, TGF- $\beta$  and WNT pathways were regulated by the miRNAs in a cell specific manner (see online supplementary figure S7). miRNAs suppressed cellular reparative response via TGF- $\beta$  and WNT signalling.

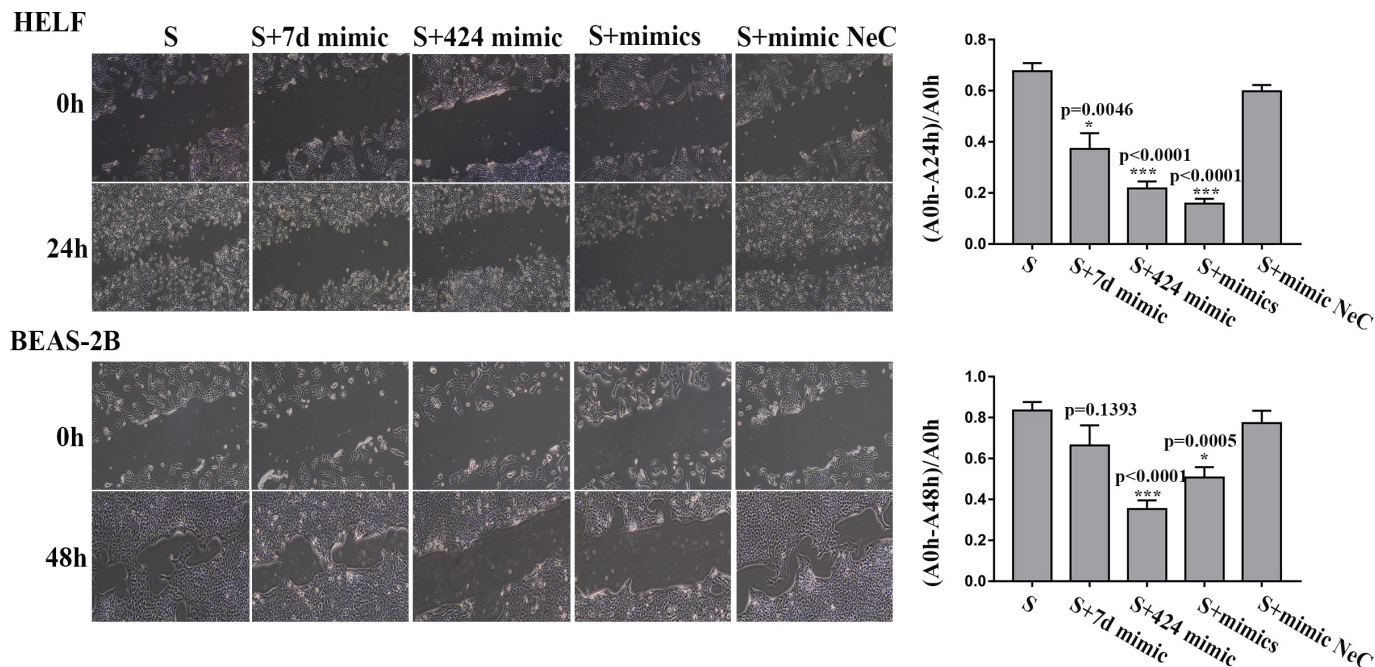


**Figure 6** Cellular wound-healing responses were suppressed by miR-424-5p or let-7d-5p. (left) Representative pictures of scratch experiments in HELF and BEAS-2B cells with miR-424-5p or/and let-7d-5p mimics. (right) Growth rate of wounded HELF and BEAS-2B cells with miR-424-5p or/and let-7d-5p mimics with at least triplicate experiments. The columns represent the means and the bars indicate SE of the means with triplicates. S represents scratch, 7d means has-let-7d-5p, 424 means has-miR-424-5p and NeC represents negative control. A0h means the area of scratch at the time of the scratch treatment, A24h means the area of scratch at the time of 24 hours later after the scratch treatment, A48h means the area of scratch at the time of 48 hours later after the scratch treatment.

To test the role of FLCN-regulated miRNAs in cellular repairing, a process involving both TGF- $\beta$  and WNT signaling,<sup>22,23</sup> we assayed cell responses to harmful stress with/without the treatment of the miRNAs mimics. In HELF cells, the scratch significantly triggered wound-healing response along the edge of damage (figure 6). Moreover, it induced  $\alpha$ -SMA expression in the insulted cells (see online supplementary figure S8), indicating an effective initiation of mesenchymal cellular reparative response and its molecular adaptation. In contrast, the administration of miR-424-5p/let-7d-5p strongly suppressed this process (figure 6 and see online supplementary figure S8). Consistently, in BEAS-2B cells, a typical epithelial cellular reparative response was also initiated on scratch and specified by cell growth and EMT response with  $\alpha$ -SMA and Slug activation and E-Cadherin reduction, which was strongly suppressed by miR-424-5p, but not let-7d-5p mimics (figure 6 and see online supplementary figure S8). The effect of the two miRNAs on wound-healing response in HELF and BEAS-2B cells were repeatable in the condition of FLCN knockdown (see online supplementary figure S9 and 10). Thus, FLCN-regulated miRNAs appeared suppressive in cellular reparative response after injury.

#### Evidence for loss of cellular reparative response was detected in PSP-BHD lesions

Finally, we validated the above cellular observations in the cystic tissues of PSP-BHD patients. As shown, a suppression of Smad7 and an activation of Smad3, as well as a decrease of FZD4 and  $\beta$ -catenin in the PSP-BHD cystic tissues were evident (figure 7A,C,F), suggesting an activation of TGF- $\beta$  and a suppression of WNT signalling in PSP-BHD lung lesions, which was consistent with the cellular findings. Moreover, the protein levels of Bim and cl.Cas3 were significantly increased

(figure 7B) and TUNEL assay detected an increased cell apoptosis in the lesion tissues (figure 7E). Moreover, an epithelial marker TJP1 was increased, while the mesenchymal indicator vimentin,  $\alpha$ -SMA and Slug were decreased in PSP-BHD lung lesions (figure 7F), indicating an MET molecular adaptation that was initially revealed in the cell studies.

To show more definitively that an overall tissue EMT configuration in the lesions of PSP-BHD tissues indeed related to the suppression of cellular reparative response, we set an immunohistochemistry study around the cystic regions. When compared with NCs, in PSP tissues, the expression of  $\alpha$ -SMA was greatly increased in a broadly distributed cells around lesion areas, whereas, the expression of TJP1 was obviously reduced in the epithelial cells (figure 7F), suggesting that given the extent of the tissue damage around cysts, the cellular reparative response was induced. However, in PSP-BHD lesions, an opposite staining pattern with greatly reduced  $\alpha$ -SMA and increased TJP1 was detected (figure 7F). Together, a loss of cellular reparative response in PSP-BHD lung lesions was suggested.

#### DISCUSSION

Spontaneous pneumothorax shared between BHDS and PSP<sup>24-27</sup> is often the first presenting manifestation<sup>28</sup> and may be the only one of BHDS,<sup>29-31</sup> whereas, the skin findings generally appear in the fourth decade of FLCN mutant carriers and become progressively more noticeable with age.<sup>32-34</sup> The renal phenotype of BHDS is also a late finding when compared with pulmonary cysts/pneumothorax.<sup>6,35</sup> Thus, the PSP-BHD is a forme fruste type of the disease,<sup>36</sup> which may confuse precise diagnosis with PSP. In fact, our previous studies and others' find<sup>2,26,29,30</sup> that spontaneous pneumothorax is the most frequently reported clinical manifestation of PSP-BHDS patients enrolled in the thoracic surgery, occupied as much as 10% of 'PSP' population.

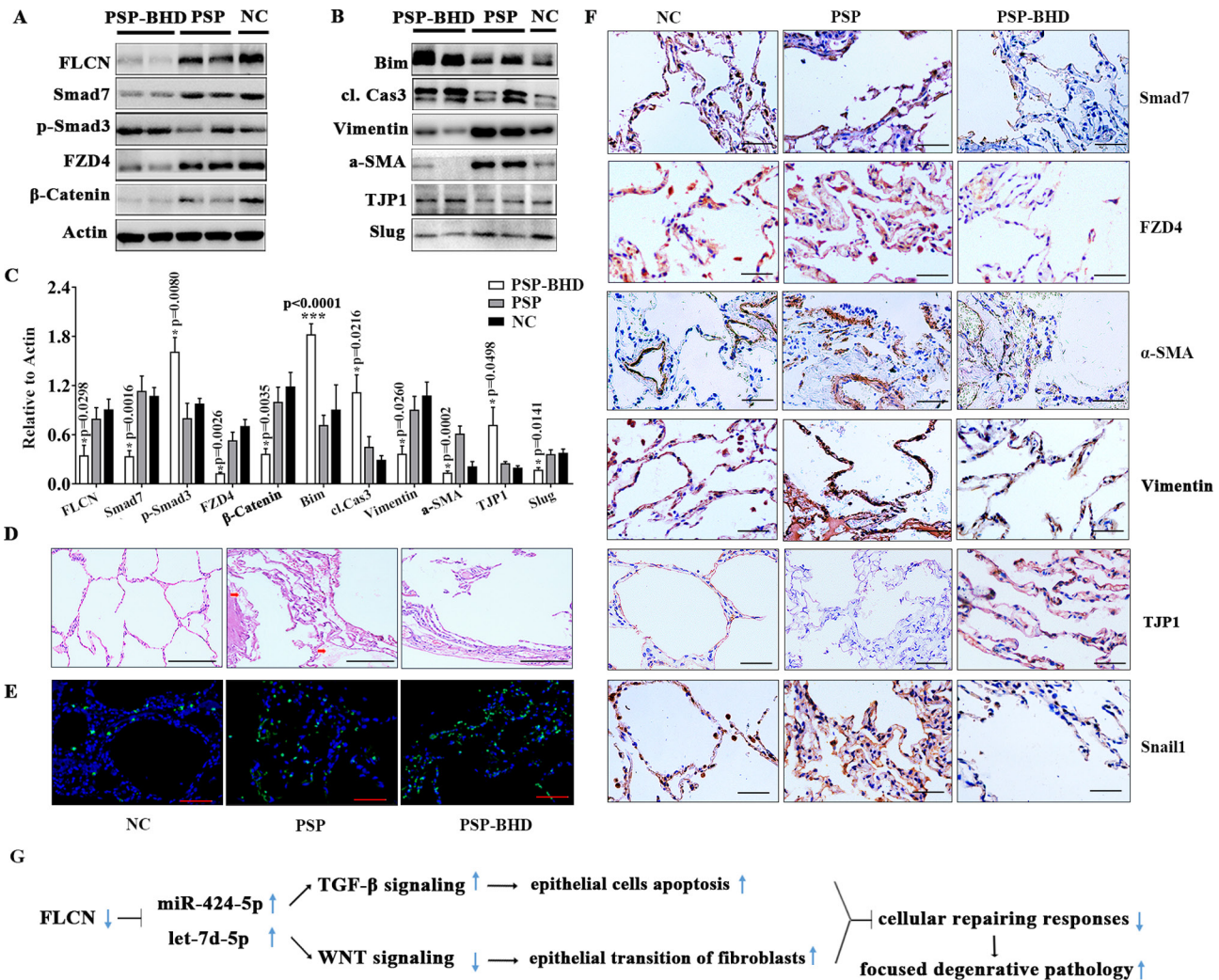


**Figure 7** Evidence for cell death and loss of cellular reparative responses in PSP-BHD lesion. (A) Proteins of TGF- $\beta$  signalling activated and WNT signalling suppressed in cystic lesions of PSP-BHD patients compared to PSP patients and cancer-free tissues (NC) lung tissues. (B) Proteins of Bim, cl.Cas3 and TJP1 upregulated and vimentin and  $\alpha$ -SMA downregulated in cystic lesions of PSP-BHD patients compared to PSP patients and controls. (C) Quantitation of proteins observed in A and B (PSP-BHD n=15, PSP n=15, NC n=9). The columns represent the means and the bars indicate standard deviation. The mutation information of PSP-BHD patients was in online supplementary table 1. (D) HE staining of lung tissue of PSP-BHD patients, PSP patients and NC. The red rows indicated exudation of the tissue. (E) Increased apoptosis observed by TUNEL in tissue section of PSP-BHD compared with that of PSP and NC. (F) Smad7, FZD4, vimentin,  $\alpha$ -SMA and Snail1 were all suppressed while TJP1 was enhanced in lesion tissue of PSP-BHD patient compared with that of PSP and NC by immunochemistry. (G) A model of cystic formation in PSP-BHD lung. The black star showed exudation. The blank line indicated 100  $\mu$ m and the red line indicated 50  $\mu$ m. BHD, clCas 3, cleaved caspase 3; FLCN, folliculin; NC, normal control; PSP, primary spontaneous pneumothorax; TGF- $\beta$ , transforming growth factor- $\beta$ ;

Thus, developing a new and cost-effective diagnostic approach for large population screen of PSP-BHD, in addition to classic genetic examination, is desirable.

In this study, we found that PSP-BHD patients showed specific miRNAs profiles compared with PSP suffers in cystic lesion and circulation, characterised by a significant and robust increase of miR-424-5p and let-7d-5p. The combination of the two delivered high diagnostic accuracy with the sensitivity at the fixed specificity of 90%. Using the combined marker, we predicted the BHDS cases in a prospective study with narrowing PSP population to 1/3 for further genetic analysis that is often central technically, unavailable for most local hospitals at least in developing regions, and costly for a large population screen. Our concept-proof study argued that miRNA detection as an initial screen may be valuable when a Mendelian syndrome with an atypical manifestation that needs to be differentiated from other

conditions that pose similar clinic appearance before a genetic analysis.

Furthermore, we also showed that miR-424-5p and let-7d-5p provided important tools in elucidating the nature of BHDS' lung pathology. Previously, studies on FLCN function revealed that BHD lungs had an increased alveolar epithelial cell apoptosis in animals and humans.<sup>15</sup> We further showed that the increased apoptosis of lung epithelial cells directly linked to the function of miR-424-5p that reduced Smad7 and enhanced Smad 3 signalling. In contrast, both miR-424-5p and let-7d-5p forced a cellular adaptation of MET via the suppression of WNT signalling in lung fibroblasts. Considering that both BEAS-2B and HELF cells expressed Smad7 and FZD4 (figure 5B and see online supplementary figure S2 and 4), as well as other tested components of WNT, TGF- $\beta$  and mTOR pathways, the miRNAs exhibited selective targeting powers in different cells with yet unknown mechanism.

Tissue studies revealed a similar molecular alteration in the BHDS lung lesions with a TGF- $\beta$  pathway activation and WNT signalling suppression. Importantly, given the extent of the lung lesion in BHDS, no reparative response was detected, instead, both normal tissue repair index EMT and myofibroblast activation<sup>22, 23</sup> were suppressed, distinguishing with non-BHDS PSP lesions that showed obvious repairing adaptation both at molecular and immunohistochemistry levels. Thus, an increased epithelium apoptosis and a weakened mesenchyme repairing may define a pathogenic condition that contributes to the development of focused degenerative cystic lesions in BHD lungs (figure 7G).

The mechanism of how FLCN might negatively regulate the miRNAs is still not known. However, a recent study shows that FLCN knockdown inhibits the motility and perinuclear clustering of lysosome,<sup>37</sup> which alters the cellular function of lysosome by increasing its PH.<sup>38</sup> Interestingly, a similar change in lysosome has been linked to the increase of exosomal secretion in cells,<sup>39</sup> indicating that FLCN deficiency may involve in hypersecretion of miRNAs, presumably in lung epithelial cells. More studies are required to deepen the mechanistic understanding of FLCN in BHDS pathology. Finally, it is acknowledged that p values of several experiments raised the possibility of type I errors (false positive), specifically in the comparisons of miR-199a-3p expression between PSP-BHD and PSP (p=0.0493) and the expression of TJP1 protein (PSP-BHD vs PSP, p=0.0498) in lung tissues (see online supplementary table 7), which may suggest the necessity for the further validation in an expanded cohort in future.

#### Author affiliations

<sup>1</sup>Jiangsu Key Laboratory for Molecular Medicine, Nanjing University Medical School, Nanjing, Jiangsu, China

<sup>2</sup>Center for Translational Medicine, Nanjing University Medical School, Nanjing, Jiangsu, China

<sup>3</sup>Department of Cardiothoracic Surgery, Taizhou Hospital of Zhejiang Province, Wenzhou Medical University, Linhai, Zhejiang, China

<sup>4</sup>Department of Thoracic Surgery, Nanjing Chest Hospital, Nanjing, Jiangsu, China

<sup>5</sup>Department of Pathology, Nanjing Chest Hospital, Nanjing, Jiangsu, China

**Acknowledgements** We would like to thank all the PSP patients and their family members who participated in the studies and the staff of Human Tissue Bank of Taizhou Hospital of Zhejiang Province for their contributions. We also thank Xicong Zhu, dermatologist at Taizhou Hospital, for dermatological examination, and candidates Lingjia Zhuang and Yu Zhang for tissue section scores.

**Funding** The study was supported by the National Natural Science Foundation of China (81570775 and 81670003), and National Key R&D Program of China (2018YFC2001800).

**Competing interests** None declared.

**Patient consent for publication** Not required.

**Ethics approval** The study was approved by the ethics committee of the two hospitals.

**Provenance and peer review** Not commissioned; externally peer reviewed.

**Data availability statement** Data are available in a public, open access repository.

**Open access** This is an open access article distributed in accordance with the Creative Commons Attribution Non Commercial (CC BY-NC 4.0) license, which permits others to distribute, remix, adapt, build upon this work non-commercially, and license their derivative works on different terms, provided the original work is properly cited, appropriate credit is given, any changes made indicated, and the use is non-commercial. See: <http://creativecommons.org/licenses/by-nc/4.0/>.

#### ORCID iD

Qian Gao <http://orcid.org/0000-0001-8189-6061>

#### REFERENCES

- Nickerson ML, Warren MB, Toro JR, *et al.* Mutations in a novel gene lead to kidney tumors, lung wall defects, and benign tumors of the hair follicle in patients with the Birt-Hogg-Dubé syndrome. *Cancer Cell* 2002;2:157–64.

- Ren H-Z, Zhu C-C, Yang C, *et al.* Mutation analysis of the FLCN gene in Chinese patients with sporadic and familial isolated primary spontaneous pneumothorax. *Clin Genet* 2008;74:178–83.
- Painter JN, Tapanainen H, Somer M, *et al.* A 4-bp deletion in the Birt-Hogg-Dubé gene (FLCN) causes dominantly inherited spontaneous pneumothorax. *Am J Hum Genet* 2005;76:522–7.
- Kunogi M, Kurihara M, Ikegami TS, *et al.* Clinical and genetic spectrum of Birt-Hogg-Dubé syndrome patients in whom pneumothorax and/or multiple lung cysts are the presenting feature. *J Med Genet* 2010;47:281–7.
- Zbar B, Alvord WG, Glenn G, *et al.* Risk of renal and colonic neoplasms and spontaneous pneumothorax in the Birt-Hogg-Dubé syndrome. *Cancer Epidemiol Biomarkers Prev* 2002;11:393–400.
- Houweling AC, Gijzen LM, Jonker MA, *et al.* Renal cancer and pneumothorax risk in Birt-Hogg-Dubé syndrome; an analysis of 115 FLCN mutation carriers from 35 BHD families. *Br J Cancer* 2011;105:1912–9.
- Toro JR, Wei M-H, Glenn GM, *et al.* BHD mutations, clinical and molecular genetic investigations of Birt-Hogg-Dubé syndrome: a new series of 50 families and a review of published reports. *J Med Genet* 2008;45:321–31.
- Menko FH, van Steensel MAM, Giraud S, *et al.* Birt-Hogg-Dubé syndrome: diagnosis and management. *Lancet Oncol* 2009;10:1199–206.
- Cacchiarelli D, Legnini I, Martone J, *et al.* miRNAs as serum biomarkers for Duchenne muscular dystrophy. *EMBO Mol Med* 2011;3:258–65.
- Liu R, Chen X, Du Y, *et al.* Serum microRNA expression profile as a biomarker in the diagnosis and prognosis of pancreatic cancer. *Clin Chem* 2012;58:610–8.
- Lu TX, Sherrill JD, Wen T, *et al.* MicroRNA signature in patients with eosinophilic esophagitis, reversibility with glucocorticoids, and assessment as disease biomarkers. *J Allergy Clin Immunol* 2012;129:1064–593.
- Gregory PA, Bracken CP, Bert AG, *et al.* MicroRNAs as regulators of epithelial-mesenchymal transition. *Cell Cycle* 2008;7:3112–7.
- Rajasekaran S, Rajaguru P, Sudhakar Gandhi PS. MicroRNAs as potential targets for progressive pulmonary fibrosis. *Front Pharmacol* 2015;6:254.
- Fabre A, Borie R, Debray MP, *et al.* Distinguishing the histological and radiological features of cystic lung disease in Birt-Hogg-Dubé syndrome from those of tobacco-related spontaneous pneumothorax. *Histopathology* 2014;64:741–9.
- Goncharova EA, Goncharov DA, James ML, *et al.* Folliculin controls lung alveolar enlargement and epithelial cell survival through E-cadherin, LKB1, and AMPK. *Cell Rep* 2014;7:412–23.
- MacDuff A, Arnold A, Harvey J, *et al.* Management of spontaneous pneumothorax: British thoracic Society pleural disease guideline 2010. *Thorax* 2010;65(Suppl 2):ii18–31.
- Paraskevopoulou MD, Georgakilas G, Kostoulas N, *et al.* DIANA-microT web server v5.0: service integration into miRNA functional analysis workflows. *Nucleic Acids Res* 2013;41:W169–73. (Web Server issue).
- Reczko M, Maragkakis M, Alexiou P, *et al.* Functional microRNA targets in protein coding sequences. *Bioinformatics* 2012;28:771–6.
- Furuya M, Tanaka R, Koga S, *et al.* Pulmonary cysts of Birt-Hogg-Dubé syndrome: a clinicopathologic and immunohistochemical study of 9 families. *Am J Surg Pathol* 2012;36:589–600.
- Jinnin M, Ihn H, Tamaki K. Characterization of SIS3, a novel specific inhibitor of Smad3, and its effect on transforming growth factor-beta1-induced extracellular matrix expression. *Mol Pharmacol* 2006;69:597–607.
- Wang H, Graves MW, Zhou H, *et al.* 2-Amino-4-(3,4-(methylenedioxy)benzylamino)-6-(3-methoxyphenyl)pyrimidine is an anti-inflammatory TLR-2, -4 and -5 response mediator in human monocytes. *Inflamm Res* 2016;65:61–9.
- Hinz B. The role of myofibroblasts in wound healing. *Curr Res Transl Med* 2016;64:171–7.
- Stone RC, Pastar I, Ojeh N, *et al.* Epithelial-Mesenchymal transition in tissue repair and fibrosis. *Cell Tissue Res* 2016;365:495–506.
- Agarwal PP, Gross BH, Holloway BJ, *et al.* Thoracic CT findings in Birt-Hogg-Dubé syndrome. *AJR Am J Roentgenol* 2011;196:349–52.
- Park HJ, Park CH, Lee SE, *et al.* Birt-Hogg-Dubé syndrome prospectively detected by review of chest computed tomography scans. *PLoS One* 2017;12:e0170713.
- Scott RM, Henske EP, Raby B, *et al.* Familial pneumothorax: towards precision medicine. *Thorax* 2018;73:270–6.
- Park HJ, Park CH, Lee SE, *et al.* Birt-Hogg-Dubé syndrome prospectively detected by review of chest computed tomography scans. *PLoS One* 2017;12:e0170713.
- Johannesma PC, Reinhard R, Kon Y, *et al.* Prevalence of Birt-Hogg-Dubé syndrome in patients with apparently primary spontaneous pneumothorax. *Eur Respir J* 2015;45:1191–4.
- Graham RB, Nolasco M, Peterlin B, *et al.* Nonsense mutations in folliculin presenting as isolated familial spontaneous pneumothorax in adults. *Am J Respir Crit Care Med* 2005;172:39–44.
- Ishii H, Oka H, Amemiya Y, *et al.* A Japanese family with multiple lung cysts and recurrent pneumothorax: a possibility of Birt-Hogg-Dubé syndrome. *Intern Med* 2009;48:1413–7.
- Xing H, Liu Y, Jiang G, *et al.* Clinical and genetic study of a large Chinese family presented with familial spontaneous pneumothorax. *J Thorac Dis* 2017;9:1967–72.

- 32 Iwabuchi C, Ebana H, Ishiko A, *et al.* Skin lesions of Birt-Hogg-Dubé syndrome: clinical and histopathological findings in 31 Japanese patients who presented with pneumothorax and/or multiple lung cysts. *J Dermatol Sci* 2018;89:77–84.
- 33 Sattler EC, Lang MU, van Steensel MAM, *et al.* Late onset of skin manifestations in Birt-Hogg-Dubé syndrome with FLCN mutation p.W260X. *Acta Derm Venereol* 2012;92:187–8.
- 34 Steinlein OK, Ertl-Wagner B, Ruzicka T, *et al.* Birt-Hogg-Dubé syndrome: an underdiagnosed genetic tumor syndrome. *J Dtsch Dermatol Ges* 2018;16:278–83.
- 35 Pavlovich CP, Grubb RL, Hurley K, *et al.* Evaluation and management of renal tumors in the Birt-Hogg-Dubé syndrome. *J Urol* 2005;173:1482–6.
- 36 Chiu HT, Garcia CK. Familial spontaneous pneumothorax. *Curr Opin Pulm Med* 2006;12:268–72.
- 37 Starling GP, Yip YY, Sanger A, *et al.* Folliculin directs the formation of a Rab34-RILP complex to control the nutrient-dependent dynamic distribution of lysosomes. *EMBO Rep* 2016;17:823–41.
- 38 Dodding MP. Folliculin - A tumor suppressor at the intersection of metabolic signaling and membrane traffic. *Small GTPases* 2017;8:100–5.
- 39 Latifkar A, Ling L, Hingorani A, *et al.* Loss of sirtuin 1 alters the secretome of breast cancer cells by impairing lysosomal integrity. *Dev Cell* 2019;49:393–408.

## Supplementary Methods

### Population

Firstly, 701 PSP patients were involved in the retrospective study with thorough skin examination, high resolution computed tomography (HRCT), abdominal and kidney ultrasonography, as well as genetic testing for FLCN mutations including Sanger sequencing and multiplex ligation-dependent probe amplification (MLPA) analysis. A total of 70 patients with FLCN germline mutations were diagnosed in the PSP population (Supplementary Table 1). Another 38 PSP patients were included in the prospective experiment without any clinical information and genetic analysis before miRNAs detecting. Finally, 4 of them were confirmed with FLCN mutations. A total of 15 healthy individuals were enrolled without current or prior history of lung diseases for plasma collection at the Center of Physical Examination of Taizhou Hospital of Zhejiang Province and 8 cancer-free lung tissue samples were obtained from 8 lung cancer patients hospitalized in Nanjing Chest Hospital.

### Sample collection

Pulmonary cystic lesions were obtained from the patients during pneumothorax surgical treatment with the intention of minimizing the excision of adjacent normal lung tissue (~1/4 of total specimens). Approximately 1/3 of each sample including cystic and adjacent tissues was fixed in 4% paraformaldehyde for IHC and H&E study. The rest of the specimen was stored in frozen for molecular analysis. In detailed, 300 mg frozen tissues including cystic and adjacent were cut, homogenized and divided into two parts (50mg for total RNA and 250 mg for protein extract). The cancer-free lung tissues used as normal controls were defined as >3cm away from cancer tissue. Approximately 5ml venous blood samples

were collected in EDTA-containing tubes and processed within 1 hour of collection. Blood samples were centrifuged at 800 g for 10 min at 4°C to spin down the blood cells, and the supernatant was transferred into RNase-free tubes, followed by a second centrifugation at 12,000 g for 10 min at 4°C. The supernatant was transferred to RNase-free tubes and stored at –80°C.

All lesions and plasmas of PSP patients were recruited from 2006 to 2015 and total RNA extraction were carried out in Jan. 2013 to Aug. 2013.

### DNA Sequencing and Bioinformatics Analysis

The human *flcn* gene is located on 17p11.2 and is encoded by 11 exons. Eleven exons of *flcn* were amplified by polymerase chain reaction (PCR) using 10 pairs of FLCN gene-specific primers designed by the Primer 3 software as following:

Primer	Sequence (5'...3')
FLCN-ex4-F	GGGAGGTTTCATGGAGTCAA
FLCN-ex4-R	CTCTCAGGTCCTCCTGTCCAT
FLCN-ex5-F	CCCTGCTTCCCAACTAACAG
FLCN-ex5-R	GCAAGTCCAACATGACTCCTC
FLCN-ex6-F	TCAGCACAGAGCGGCTCATG
FLCN-ex6-R	GAAGAGGCTTTGATTTGGTGTCAC
FLCN-ex7-F	GCATGGAGAGAGTATAGTGGGACT
FLCN-ex7-R	GCCAACCAATGTATCGTGACT
FLCN-ex8-F	AGGGAACCACTGCCCTTCAT
FLCN-ex8-R	TCAGGTTTGCTTTTTCCTTTGG
FLCN-ex9-F	CCATGAAGTATCTTGGGCTGA
FLCN-ex9-R	GAGGCTGTCAGTCACTTCCTG
FLCN-ex10-F	GTCTTTCTCCTGAGCCCTGTC
FLCN-ex10-R	CAGTGGAGACCGTGTGGTG
FLCN-ex11-F	GGTTTGGGTAGTAGAGCATGGA

---

FLCN-ex11-R	CAGAGATCTGGTTCCACTTTGG
FLCN-ex1213-F	CAGCTCCAGGTTTTCTCCAGG
FLCN-ex1213-R	CACGGTGGGCTAGCGCAG
FLCN-ex14-F	ACCAGGGCTCGAGGGATTG
FLCN-ex14-R	TGTCTTTAGGCAGGTGTGTGTGA

---

PCR fragments were purified with Gel Extraction Kit (Omega), subjected to cycle sequencing using BigDye Terminator v3.1 Kit and injected to ABI 3100 Genetic Analyzer (Applied Biosystems).

Variation sites were identified by referring to FLCN gene sequence derived from GenBank (accession number: NG\_008001.2). Altered nucleotides were confirmed by sequencing from the other strand. The novelty of all variants found was determined from the National Center for Biotechnology Information (NCBI) human SNP database (dbSNP), the 1000 Genome Project database and Exome Sequencing Project (ESP).

#### **Multiplex Ligation-Dependent Probe Amplification Assay (MLPA)**

Two MLPA kits were used to detect deletions/duplications in a genomic region of the 25 kb FLCN gene, 9kb upstream and 5kb downstream. The commercial kit, SALSA MLPA Kit P256-B1 FLCN (MRC Holland, Netherlands), contained 26 probes, including 14 probes for the 14 exons respectively, 2 mutation specific probes for hypermutable C8 tract in exon 11, and 9 reference probes. Besides that, we synthesized another MLPA kit by following the guidelines from MRC-Holland, in which 15 probes pairs were designed to target the region around the FLCN gene, 9 for the upstream and 6 for the downstream. MLPA reactions were performed following provider's instructions, and products were analyzed on an ABI 3130 Genetic Analyzer. Data were collected and evaluated with the GeneMapper software (Applied Biosystems).

**Cell lines culture**

BEAS-2B, A549, HaCaT and HEK293 cells were cultured in DMEM containing 4.5g/L D-Glucose (Gibco) supplemented with 10% FBS (Hyclone) in the condition of 37°C, 5% CO<sub>2</sub>. HELF cells were cultured in DMEM containing 4.5g/L D-Glucose (Gibco) supplemented with 8% NCS (Hyclone) in the condition of 37°C, 5% CO<sub>2</sub>. In apoptosis detecting experiments, BEAS-2B cells were firstly stressed in DMEM containing 4.5g/L D-Glucose (Gibco) supplemented with 2% FBS (Hyclone) for 24 hours.

**Knockdown and overexpress of FLCN**

Knockdown of FLCN in BEAS-2B, HaCaT, HEK293 and HELF cells cultured in 6-well plates was carried out at the time of 80-90% confluent.

The detailed procedure was as follow:

1) 20nmole duplex siRNA (Invitrogen) was suspended in 1ml RNase-free water to make a 20μM solution. Stealth RNAi siRNA sequence:

5' to 3' GAACACAGCCUUCACGCCAUUCCUA

5' to 3' UAGGAAUGGCGUGAAGGCUGUGUUC

2) 5ul RNAi Max Reagent (Invitrogen) was diluted in 145ul Opti-MEM™ Medium (Invitrogen), incubated for 5 minutes at room temperature.

3) Volume of siRNA and Opti-MEM Medium used in 4 types of cell lines were as follow: BEAS-2B cells, 10ul + 140ul; HaCaT cells, 15ul + 135ul; HEK293 cells, 10ul + 140ul; HELF cells, 15ul + 135ul.

4) Dilution of RNAi Max Reagent and siRNA were mixed to be incubated for 20 minutes at room temperature.

- 5) The mixture was added into a well of the 6-well plate.
- 6) Cells were incubated at 37°C, 5% CO<sub>2</sub>, 24 hours for RNA extraction and 48 hours for protein extraction.

Transfection of FLCN wildtype- and mutant-overexpressed vectors in A549 cells cultured in 6-well plate were carried out at the time of about 80-90% confluent. The detailed procedure was as follow:

- 1) Dilute 4 ul Lipofectamine™ 3000 Reagent in 125 ul Opti-MEM™ Medium.
- 2) Dilute 3ug DNA in 125 ul Opti-MEM™ Medium (Invitrogen), and then add 6ul P3000™ Reagent into the DNA dilution.
- 3) Mix the dilution of Lipofectamine™ 3000 Reagent and DNA and incubate for 15min at room temperature.
- 4) Add the mixture into a well of 6-well plate and incubate plates at 37°C, 5% CO<sub>2</sub>, 24 hours for RNA extraction and 48 hours for protein extraction.

#### **Mimics and inhibitor of miRNAs transfection**

The control and mimics and inhibitor of miRNAs were synthesized by Invitrogen and the sequences were as follow:

hsa-let-7d-5p mimic

5' to 3' AGAGGUAGUAGGUUGCAUAGUU

5' to 3' CUAUGCAACCUACUACCUCUUU

hsa-miR-424-5p mimic

5' to 3' CAGCAGCAAUUCAUGUUUUGAA

5' to 3' CAAAACAUGAAUUGCUGCUGUU

Negative control of mimics

5' to 3' UUCUCCGAACGUYUCACGUTT

5' to 3' ACGUGACACGUUCGGAGAATT

Inhibitor of miR-424-5p

5' to 3' UUCAAAACAUGAAUUGCUGCUG

Control of inhibitor

5' to 3' CAGUACUUUUGUGUAGUACAA

The procedure of miRNAs mimics/inhibitor (100nmol) transfected was as the same as that of siRNA transfection. Signaling pathways reagents are SIS3 (MCE), an inhibitor of phospho-Smad3, and BML-284 (MCE), an activator of WNT signaling.

### **Primers in mRNA detection**

All primers were synthesized by GenScript Biotech Corporation. Sequences of primers are as follow

Actin forwards 5'CATCCGCAAAGACCTGTACG3', reverse 5'CCTGCTTGCTGATCCACATC3';

Vimentin forwards 5'GAGAGGAAGCCGAAAACACC3', reverse 5'TTCCTGAATCTGAGCCTGCA3';

TJP1 forwards 5'CTAAACCTGGGGCTGTCTCA3', rewards 5'AATTCATGCTGGGCCGAAG3';

$\alpha$ -SMA forwards 5'GAGAAGAGTTACGAGTTGCCTGA3', rewards 5'TGTTAGCATAGAGGTCCTTCCTG3';

Slug forwards 5'CTGCGGCAAGGCGTTTTCCAGA3', rewards 5'CAGATGAGCCCTCAGATTTGAC3';

E-Cadherin forwards 5'TGCCCAGAAAATGAAAAGG3', rewards 5'GTGTATGTGGCAATGCGTTC3'.

#### **miRNAs assay and reverse transcription quantitative PCR analysis**

Total RNA containing miRNAs was extracted with miRNeasy Mini Kit (Qigen) from 20mg frozen lung cystic lesions or  $1 \times 10^6$  cultured cells. Plasma miRNAs were extracted with mirVana PARIS (Ambion) from 400ul samples, mixed with 100pmol/L synthesized cel-miR-39 as internal calibrators to monitor extracted efficiency and as external reference. The Universal ProbeLibrary (UPL) assays (Roche) were used for tissue miRNAs screen. The selection criterion of miRNAs was consisted of the value of CT < 35 and up/down-regulated consistently. Reverse transcription was completed with PrimeScript RT-PCR Kit (Takara). qPCR of miRNAs or mRNA was performed with UPL probe kit (Roche) or sybreen mix (Invitrogen) according to their instructions.

#### **Antibodies and Western bolt**

Proteins were extracted from 30mg lung tissues and  $1 \times 10^6$  cultured cells by RIPA lysis buffer on ice. Concentration of protein was detected by a BCA protein kit (Pierce). 50 $\mu$ g protein of each sample was resolved on 10% sodium dodecyl sulfate polyacrylamide gel electrophoresis buffer, transferred to PVDF membrane and detected by indicated antibodies. The detailed information of antibodies are rabbit monoclonal FLCN (CST),

1:1000; rabbit monoclonal  $\beta$ -actin (CST), 1:1000; rabbit monoclonal Smad3 (CST), 1:1000; rabbit monoclonal phospho-Smad3 (Ser423/425) (CST), 1:1000; rabbit polyclonal Cleaved Caspase-3(CST), 1:1000; rabbit monoclonal Bim (CST), 1:1000; rabbit monoclonal Smad7/MADH7 (Epitomics), 1:500; Epithelial-Mesenchymal transition antibody sampler Kit (CST), 1:1000; rabbit monoclonal TSC2 (CST), 1:1000; rabbit monoclonal mTOR (7C10) (CST), 1:1000; frizzled-4 (C-18):sc-66459 (santa cruz),1;100; alpha-actin (smooth muscle) E184 (abcam), 1;1000.

### **Annexin V-FITC/PI staining**

BEAS-2B cells cultured in 6-well plates for transfection of siFLCN vs scFLCN, miR-424-5p mimic vs mimic control, siFLCN+ miR-424-5p inhibitor vs siFLCN+ inhibitor control. 48 hours later, cells were harvested and stained with AnnexinV-FITC and propidium iodide. And then cells were assessed for the percentage of double-negative population using a Calibur flow cytometer (BD). Data were analyzed using FlowJo Version 7.6.2 software (TreeStar).

### **Luciferase reporter assays**

The segment sequence of the Smad7 3' UTR (100bp) that contained the putative miR-424-5p binding sequence and FZD4 3' UTR (100bp) that contained the putative let-7d-5p and miR-424-5p binding sequences were amplified and subcloned into dual-luciferase reporter vectors (Promega) to generate the pGL3-promoter-Smad7-WT reporter and pGL3-promoter-FZD4-WT (Realgene). The pGL3-promoter-Smad7-MU reporter was achieved by changing the miR-424-5p binding seed sequence from ACGACGA to AGGUCCA and pGL3-promoter-FZD4-MU were achieved by changing the miR-424-5p binding seed sequence from UGCUGCU to UGGUCCA and let-7d-5p binding seed sequence from CUACCUC to

GGUUGCG respectively.

HEK293 cells were seeded in 24-well plates one day before transfection and then co-transfected with WT or MU constructs and mimics or mimic control duplexes using Lipofectamine 3000 reagent (Life technology). After 48 hours, luciferase activity analysis was used by a Dual-Luciferase Assay System Kit (Promega).

### **Hematoxylin and eosin (H&E) staining and Immunohistochemistry-Paraffin**

The cystic lesions were fixed with 4% paraformaldehyde and embedded in paraffin. 7 $\mu$ m tissue sections were prepared for H&E staining and Immunohistochemistry examinations. Immunohistochemistry was performed by standard protocol. Briefly, the tumor sphere was removed from implanted region and fix with 4% paraformaldehyde and embedded in paraffin. After hydrolysis and antigen retrieval, the slides of both tumor bearing mouse and human patients were blocked and washed with PBS. Immunostaining was carried out with rabbit monoclonal antibody to Smad7, FZD4, Vimentin,  $\alpha$ -SMA (Abcam), TJP1 (CST) and Snail (Proteintech) at 4°C overnight.

### **TUNEL**

DNA damage was determined using TUNEL assay with in situ Cell Death Detection Fluorescein Kit. The kit reagents detect damaged cells in situ by specific end labeling and detection of DNA fragments produced by the apoptotic process. The tissue sections were deparaffinized with a standard histological protocol, permeabilized with Triton X-100 at 4 °C for 2 min, and then flooded with TdT enzyme and reaction buffer for 60 min at 37°C, followed by direct analysis with a FV10i Laser Scanning Confocal Microscope (Olympus, Center Valley, PA, USA) to determine

the degree of apoptosis. Negative controls were performed by substituting PBS for TdT enzyme in the preparation of working solutions. Positive controls were prepared by treating sections with DNase I for 10 min at room temperature before detection.

## **Supplementary Tables**

Supplementary Table 1 Clinical and FLCN gene mutation informations of PSP patients.

Supplementary Table 2 Summary of characteristics of patients and control subjects.

Supplementary Table 3 A stepwise linear regression by SPSS17.0 to analyze the associations between varied factors and expressions of miRNAs.

Supplementary Table 4 Fold change of differentially-expressed miRNAs in cystic lesions of BHD-PSP compared with that of nB-PSP patients via miRNA assays.

Supplementary Table 5 Signaling pathways and biological process interacted with miRNAs dysregulated in cystic lesions of BHD-PSP by DIANA-mirPath analysis.

Supplementary Table 6 The optimal signaling pathways and targets of miR-424 and let-7d predicted by DIANA-mirPath.

Supplementary Table 7 p values of all figures were stasitically calculated by students' T test.

Supplementary Table 1

Stage	Patient ID	Sex	Age <sup>a</sup>	Affected family members	Number of episodes	Distribution of cysts <sup>b</sup>	Mutant exon	Mutation type	Protein change	Report status
Screen of miRNAs	F275	M	42(41)	6	1	Bi, U & L	9	Frameshift	p.S316YfsX73	This study
	F288	M	47(NA <sup>c</sup> )	1	0	Bi, U & L	14	Frameshift	p.R527QfsX75	Furuya M et al. 2012
	F305	M	29(28)	0	3	Bi, U & L	11	Frameshift	p.H429PfsX27	Nickerson et al. 2002
	F627	M	43(39)	0	1	Bi, U- apical	Null	Null	Null	Null
	F636	M	25(21)	0	1	Bi, U- apical	Null	Null	Null	Null
	F711	M	24(22)	0	2	Un, U- apical	Null	Null	Null	Null
Stage	Patient ID	Sex	Age <sup>a</sup>	Affected family members	Number of episodes	Distribution of cysts <sup>b</sup>	Mutant exon	Mutation type	Protein change	Report status
Validation of miRNAs (tissue)	F297	M	55(45)	1	2	Bi, U & L	14	Frameshift	p.R527QfsX75	Furuya M et al. 2012
	F791	F	54(42)	0	2	Bi, U & L	11	Frameshift	p.H429TfsX39	Nickerson et al. 2002
	F634	F	40(36)	1	1	Un, U & L	10	Frameshift	p.S386DfsX63	Ren et al. 2008
	F641	M	65(NA)	0	NA	Bi, U	6	In-frame deletion	p.F157del	Ren et al. 2008
	F647	F	31(31)	0	0	Un, U	6	In-frame deletion	p.F157del	Ren et al. 2008
	F304	F	64(63)	0	2	Bi, L	12	Frameshift	p.C454LfsX2	This study
	F610	M	45(40)	3	2	Bi, U & L	6	In-frame deletion	p.F157del	Ren et al. 2008
	F721	M	49(44)	0	1	Bi, U & L	4	Frameshift	p.P63TfsX69	This study
	F734	F	53(48)	0	1	Bi, U & L	11	Frameshift	p.H429TfsX39	Nickerson et al. 2002
	F729	F	46(25)	0	2	Bi, U & L	11	Frameshift	p.E434VfsX21	This study
	F665	M	30(18)	1	2	Un, U & L	11	Frameshift	p.H429TfsX39	Nickerson et al. 2002
	F611	F	38(36)	0	1	Bi, U & L	10	Frameshift	p.S386DfsX63	Ren et al. 2008
	F728	M	56(39)	1	2	Bi, U & L	11	Frameshift	p.(His429Thrfs)	Nickerson et al.

Stage	Patient ID	Sex	Age <sup>a</sup>	Affected family members	Number of episodes	Distribution of cysts <sup>b</sup>	Mutant exon	Mutation type	Protein change	Report status
	F751	M	41(39)	0	1	Bi, U & L	6	In-frame deletion	p.F157del	Ren et al. 2008
	F339	M	18	0	1	Bi, U	Null	Null	Null	Null
	F341	M	19(18)	0	3	Un, U-apical	Null	Null	Null	Null
	F347	M	18(17)	0	1	Un, U-apical	Null	Null	Null	Null
	F360	M	21(21)	0	1	Un, U-apical	Null	Null	Null	Null
	F486	M	17(15)	0	3	Bi, U & L	Null	Null	Null	Null
	F988	M	18(17)	0	3	Bi, U	Null	Null	Null	Null
	F370	M	17(16)	0	3	Bi, U	Null	Null	Null	Null
	F682	F	66(60)	0	2	Bi, U & L	Null	Null	Null	Null
	F616	M	24(19)	0	1	Un, U	Null	Null	Null	Null
	F685	M	65(60)	0	1	Bi, U	Null	Null	Null	Null
	F659	M	72(69)	0	1	Un, U-apical	Null	Null	Null	Null
	F604	F	30(25)	0	1	Un, U-apical	Null	Null	Null	Null
	F603	M	38(33)	0	1	Un, U-apical	Null	Null	Null	Null
	F602	M	50(36)	0	2	Bi, U	Null	Null	Null	Null
Detection of miRNAs (plasma)	F260	F	32 (29)	2	2	Un, L- basal	1-3	Large intragenic deletion	NA <sup>c</sup>	Ding et al. 2015
	F721	M	49(44)	0	1	Bi, U & L	4	Frameshift	p.P63TfsX69	This study
	F789	F	45(43)	3	1	Bi, U-apical,L-basal	4	Frameshift	p.P63TfsX69	This study
	F047	F	48 (39)	3	2	Un,U & L	6	In-frame deletion	p.F157del	Ren et al. 2008
	F610	M	45(40)	3	2	Bi, U & L	6	In-frame deletion	p.F157del	Ren et al. 2008
	F473	M	46(46)	0	1	Un, U-apical & L	6	In-frame deletion	p.F157del	Ren et al. 2008
	F903	F	73(51)	2	2	Bi, U & L	6	In-frame deletion	p.F157del	Ren et al. 2008
	F909	M	41(41)	4	1	Bi, U & L	6	In-frame deletion	p.F157del	Ren et al. 2008
	F885	F	62(56)	0	4	Bi, U & L	6	Nonsense	p.W169X	This study
	F437	F	56 (55)	0	1	Bi, U & L	6	Frameshift	p.I158TfsX19	This study
	F465	M	29(29)	0	1	Un, apical & L	9-14	Large intragenic	NA <sup>c</sup>	Ding et al.

							deletion		2015
F753	M	45(36)	0	2	Bi, U & L	9-14	Large intragenic deletion	NA <sup>c</sup>	Ding et al. 2015
F465	M	29(29)	0	1	Un, apical	9-14	Large intragenic deletion	NA <sup>c</sup>	Ding et al. 2015
F109	M	44(36)	2	2	Un, U & L	9-14	Large intragenic deletion	NA <sup>c</sup>	Ding et al. 2015
F805	F	52(46)	2	2	Bi, U & L	9-14	Large intragenic deletion	NA <sup>c</sup>	Ding et al. 2015
F953	F	38(38)	1	2	Un, U	9	Nonsense	p.S296X	This study
F275	M	42(41)	6	1	Bi, U & L	9	Frameshift	p.S316YfsX73	This study
B217	F	23(20)	0	3	Bi, U & L	9	Frameshift	p.P326PfsX64	This study
B085	M	44(44)	0	1	Un, U & L	9	Frameshift	p.Q339SfsX13	This study
F608	M	43(42)	3	1	Bi, U & L	10	Frameshift	p.S386DfsX63	Ren et al. 2008
F634	F	40(36)	1	1	Un, U & L	10	Frameshift	p.S386DfsX63	Ren et al. 2008
F611	F	38(36)	0	1	Bi, U & L	10	Frameshift	p.S386DfsX63	Ren et al. 2008
B239	M	59 (54)	0	5	Bi, U & L-basal	10	In-frame insertion	p.H383ins	This study
F894	M	34(24)	1	3	Bi, U & L	11	Frameshift	p.H429TfsX27	Nickerson et al. 2002
F899	F	50(50)	2	1	Bi, U & L	11	Frameshift	p.H429TfsX27	Nickerson et al. 2002
F954	M	40(40)	0	1	Un,U & L	11	Frameshift	p.H429TfsX27	Nickerson et al. 2002
F466	F	29(29)	0	1	Bi, U & L	11	Frameshift	p.H429TfsX27	Nickerson et al. 2002
F665	M	30(18)	1	2	Un, U & L	11	Frameshift	p.H429TfsX39	Nickerson et al. 2002
F734	F	53(48)	0	1	Bi, U & L	11	Frameshift	p.H429TfsX39	Nickerson et al. 2002
F749	M	58(56)	0	1	Bi, U & L	11	Frameshift	p.H429TfsX39	Nickerson et al.

										2002
F758	M	25(22)	2	1	Un, L- basal	11	Frameshift	p.H429TfsX39		Nickerson et al. 2002
F161	F	72(32)	4	4	Bi, U & L	11	Frameshift	p.I426IfsX30		This study
B213	F	48(45)	0	2	Un, U & L	12	Nonsense	p.Y463X		This study
F372	M	43(40)	0	2	Bi, U & L	14	Frameshift	p.R527QfsX75		Furuya M et al. 2012
F854	F	33(33)	4	1	Un, U & L	14	Frameshift	p.R527QfsX75		Furuya M et al. 2012
F396	M	66(66)	0	2	Bi, U & L	14	Frameshift	p.L550DfsX48		This study
F604	F	30(25)	0	1	Un, U	Null	Null	Null		Null
F635	M	24(20)	0	1	Un, U	Null	Null	Null		Null
F654	M	24(20)	0	3	Un, U	Null	Null	Null		Null
F676	M	24(19)	0	1	Un, U	Null	Null	Null		Null
F277	M	22(18)	0	2	Un, U	Null	Null	Null		Null
F291	M	29(28)	0	1	Un, U	Null	Null	Null		Null
F292	M	23(22)	0	1	Un, U	Null	Null	Null		Null
F720	M	29(24)	0	1	Un, U-apical	Null	Null	Null		Null
F878	M	15(15)	0	1	Un, U-apical	Null	Null	Null		Null
F456	M	32(32)	0	2	Un, U-apical	Null	Null	Null		Null
F468	M	24(24)	0	1	Un, U-apical	Null	Null	Null		Null
F289	F	23(21)	0	2	Un, U-apical	Null	Null	Null		Null
F893	M	23(20)	0	1	Un, U-apical	Null	Null	Null		Null
F902	M	23(23)	0	1	Un, U-apical	Null	Null	Null		Null
F918	M	18(18)	0	1	Un, U-apical	Null	Null	Null		Null
F674	M	31(26)	0	2	Un, U	Null	Null	Null		Null
F263	M	21(18)	0	2	Un, U-apical	Null	Null	Null		Null
F252	M	18(16)	0	1	Un, U-apical	Null	Null	Null		Null
F416	M	17(17)	0	3	Un, U-apical	Null	Null	Null		Null
F262	M	20(16)	0	4	Un, U-apical	Null	Null	Null		Null

F265	M	24(22)	0	1	Un, U-apical	Null	Null	Null	Null
F259	M	19(16)	0	2	Un, U-apical	Null	Null	Null	Null
F710	M	16(14)	0	1	Un, U-apical	Null	Null	Null	Null
F483	M	18(18)	0	1	Un, U-apical	Null	Null	Null	Null
F452	M	18(18)	0	1	Un, U-apical	Null	Null	Null	Null
F616	M	24(19)	0	1	Un, U	Null	Null	Null	Null
F496	M	26(26)	0	1	Un, U	Null	Null	Null	Null
F486	M	17(15)	0	3	Bi, U & L	Null	Null	Null	Null
F638	M	57(57)	0	1	Bi, U & L	Null	Null	Null	Null
B216	M	50(50)	0	1	Bi, U & L	Null	Null	Null	Null
B218	F	43(42)	0	2	Un, U & L	Null	Null	Null	Null
B240	M	18(18)	0	2	Un, U & L	Null	Null	Null	Null
F432	M	17(17)	0	2	Un, U-apical & L	Null	Null	Null	Null
F436	M	25(25)	0	1	Un, U & L	Null	Null	Null	Null
F448	M	21(21)	0	1	Un, U & L	Null	Null	Null	Null
F481	M	49(49)	0	1	Un, U & L	Null	Null	Null	Null
F280	M	33(24)	0	2	Bi, U & L	Null	Null	Null	Null
F290	M	49(48)	0	1	Bi, U & L	Null	Null	Null	Null
F321	M	59 (59)	0	1	Bi, U & L	Null	Null	Null	Null
F334	M	17(15)	0	1	Un, U-apical & L-basal	Null	Null	Null	Null
F336	M	19(15)	0	5	Bi, U & L	Null	Null	Null	Null
F692	M	24(19)	0	1	Un, U & L	Null	Null	Null	Null
F607	M	36(31)	0	1	Un, U & L	Null	Null	Null	Null
F788	M	52(52)	0	1	Un, U & L	Null	Null	Null	Null
F678	M	25(20)	0	2	Bi, U & L	Null	Null	Null	Null
F931	M	19(18)	0	2	Un, U & L	Null	Null	Null	Null
F872	M	23(23)	0	1	Un, U & L	Null	Null	Null	Null
F886	M	23(21)	0	3	Bi, U & L	Null	Null	Null	Null
F873	F	37(37)	0	1	Un, U & L	Null	Null	Null	Null

	F266	M	51(51)	0	1	Bi, U & L	Null	Null	Null	Null
	F269	M	17(17)	0	1	Un, L- basal	Null	Null	Null	Null
	F270	M	36(36)	0	1	Un, L	Null	Null	Null	Null
	F250	M	19(15)	0	2	Bi, U & L	Null	Null	Null	Null
	F458	M	22(20)	0	2	Un,U & L	Null	Null	Null	Null
	F486	M	17(17)	0	3	Bi, U & L	Null	Null	Null	Null
	F612	M	35(32)	0	1	Bi, U & L	Null	Null	Null	Null
	F714	M	47(47)	0	1	Bi, U & L	Null	Null	Null	Null
Stage	Patient ID	Sex	Agea	Affected family members	Number of episodes	Distribution of cystsb	Mutant exon	Mutation type	Protein change	Report status
Observation of molecular events (tissue)	F345	M	61(59)	1	2	Bi, U & L	1-3	Large intragenic deletion	NA <sup>c</sup>	Ding et al. 2015
	F419	M	24(19)	0	2	Un, U	9	Frameshift	p.S316YfsX73	This study
	B217	F	23(20)	0	3	Bi, U & L	9	Frameshift	p.P326PfsX64	This study
	B279	M	57(56)	0	2	Bi, U & L	14	Splicesite	NA <sup>c</sup>	This study
	B268	M	42(NA)	NA	NA	Bi, U & L	13	In-frame deletion	p.K508del	So et al. 2009
	B270	F	50(49)	0	1	Un, U & L	11	Frameshift	p.H429TfsX39	Nickerson et al. 2002
	B261	M	25(24)	0	1	Bi, U & L	9	Frameshift	p.S316YfsX73	This study
	B239	M	59(54)	0	5	Bi, U & L-basal	10	In-frame insertion	p.H383ins	This study
	B213	F	48(45)	0	2	Un, U	12	Nonsense	p.V473X	This study
	B085	M	44(44)	0	1	Bi, U & L	9	Frameshift	p.Q339SfsX13	This study
	B081	M	66(34)	0	4	Un, U	Null	Null	Null	Null
	B080	M	19(16)	0	3	Un, U	Null	Null	Null	Null
	B076	M	26(26)	0	1	Un, U- apical	Null	Null	Null	Null
	B087	M	59(59)	0	1	Un, U	Null	Null	Null	Null
	B079	M	47(47)	0	1	Bi, U	Null	Null	Null	Null
	F867	M	64(64)	0	2	Bi, U&L	Null	Null	Null	Null
	F870	M	29(27)	0	1	Un, U- apical	Null	Null	Null	Null
	F869	M	50(50)	0	1	Un, U	Null	Null	Null	Null

B077	F	59(50)	0	3	Un, U- apical	Null	Null	Null	Null
B086	M	21(18)	0	2	Un, U- apical	Null	Null	Null	Null

<sup>a</sup> Age (years) at enrollment in the study is shown. Age at the first PSP episode is indicated in parentheses.

<sup>b</sup> Distribution of cysts, Un is abbreviated of Unilateral lung cysts; Bi is abbreviated of Bilateral lung cysts; U is abbreviated of Upper; L is abbreviated of lower.

<sup>c</sup> NA,not applicable

**Supplementary Table 2**

	Validation of miRNAs (plasma)				Observation of molecular events (tissue) N=8
	PSP-BHD N=36	PSP N=57	Normal control N=15		
Mean of Age (SD)	44(13)	28(12)	50 (6)	P<0.0001	66 (10)
Female/Male	17/19	4/53	7/8	P<0.0001	3/5
Status of lung disease	BHDS	PSP	None		Lung cancer (cancer-free tissues were >3cm away from cancer focus)

**Supplementary Table 3**

Model <sup>a</sup>	Unstandardized Coefficients		Standardized Coefficients	t	Sig.	Model <sup>b</sup>	Unstandardized Coefficients		Standardized Coefficients	t	Sig.
	B	Std. Error	Beta				Beta	B	Std. Error		
(Constant)	0.031	0.004		8.837	0.000	(Constant)	22.725	1.272		17.869	0.000
mutation	-0.025	0.004	-0.495	-5.869	0.000	mutation	-17.878	1.558	-0.744	-11.479	0.000

a. Dependent Variable: miR424

b. Dependent Variable: let7d

**Supplementary Table 4**

Up-regulated miRNAs				Down-regulated miRNAs			
order	name	Fold	SD	order	name	Fold	SD
1	hsa-miR-199a-3p	23.22	7.85	1	hsa-miR-628-5p	0.04	0.02
2	hsa-let-7d	18.86	11.03	2	hsa-miR-23b	0.11	0.09
3	hsa-miR-424	10.54	0.72	3	hsa-miR-26a	0.14	0.12
4	hsa-miR-194	7.819	3.56	4	hsa-miR-155	0.14	0.12
5	hsa-miR-19b	5.422	4.21	5	hsa-miR-193a-3p	0.15	0.17
6	hsa-miR-195	4.988	2.04	6	hsa-miR-30c	0.15	0.09
7	hsa-miR-125b	4.255	3.37	7	hsa-miR-192	0.16	0.07
8	hsa-miR-375	3.561	1.72	8	hsa-miR-412	0.16	0.09
9	hsa-miR-455-3p	3.501	1.17	9	hsa-miR-450b-3p	0.19	0.12
10	hsa-miR-483-5p	3.208	1.47	10	hsa-miR-532-5p	0.20	0.13
11	hsa-miR-130a	2.385	0.61	11	hsa-miR-376b	0.20	0.20
				12	hsa-miR-518d-3p	0.20	0.16
				13	hsa-miR-448	0.21	0.12
				14	hsa-miR-494	0.21	0.15
				15	hsa-miR-885-3p	0.22	0.13
				16	hsa-miR-496	0.22	0.15
				17	hsa-miR-515-3p	0.22	0.13
				18	hsa-miR-10b	0.22	0.12
				19	hsa-miR-495	0.22	0.15
				20	hsa-miR-651	0.23	0.14
				21	hsa-miR-654-3p	0.23	0.15
				22	hsa-miR-520b	0.24	0.14
				23	hsa-miR-512-5p	0.24	0.15
				24	hsa-miR-509-3-5p	0.24	0.13
				25	hsa-miR-671-3p	0.25	0.14
				26	hsa-miR-489	0.25	0.13
				27	hsa-miR-525-5p	0.25	0.17
				28	hsa-miR-892a	0.25	0.17
				29	hsa-miR-889	0.25	0.15
				30	hsa-miR-888	0.25	0.15
				31	hsa-miR-423-5p	0.25	0.14
				32	hsa-miR-342-3p	0.25	0.10
				33	hsa-miR-561	0.26	0.17
				34	hsa-miR-493	0.26	0.16
				35	hsa-miR-20a	0.26	0.19
				36	hsa-miR-518a-3p	0.26	0.17
				37	hsa-miR-509-5p	0.26	0.19
				38	hsa-miR-660	0.27	0.18
				39	hsa-miR-891b	0.27	0.19
				40	hsa-miR-890	0.27	0.17
				41	hsa-miR-510	0.28	0.18

42	hsa-miR-487b	0.28	0.18
43	hsa-miR-506	0.28	0.11
44	hsa-miR-422a	0.28	0.16
45	hsa-let-7e	0.29	0.17
46	hsa-miR-524-5p	0.29	0.13
47	hsa-miR-652	0.29	0.05
48	hsa-miR-508-5p	0.30	0.17
49	hsa-miR-629	0.30	0.13
50	hsa-miR-485-5p	0.31	0.14
51	hsa-miR-526b	0.34	0.08
52	hsa-miR-574-3p	0.36	0.07

**Supplementary Table 5**

KEGG pathway	Interacted miRNAs	p-value
Glioma	25	0
Ubiquitin mediated proteolysis	24	0
<b>Wnt signaling pathway</b>	24	0
<b>ErbB signaling pathway</b>	23	0
<b>TGF-beta signaling pathway</b>	23	0
<b>MAPK signaling pathway</b>	22	0
<b>PI3K-Akt signaling pathway</b>	22	0
Axon guidance	21	0
<b>mTOR signaling pathway</b>	21	5.55E-16
Pathways in cancer	20	0
Transcriptional misregulation in cancer	20	6.25E-14
Endocytosis	19	0
Neurotrophin signaling pathway	19	0
Prostate cancer	19	0
Hepatitis B	19	4.09E-13
Insulin signaling pathway	18	1.11E-16
Endometrial cancer	18	2.01E-09
Non-small cell lung cancer	18	3.13E-09
Dopaminergic synapse	17	3.46E-07
Acute myeloid leukemia	17	8.56E-05
Focal adhesion	16	0
Chronic myeloid leukemia	16	5.63E-14
Long-term potentiation	16	1.20E-10
Melanoma	16	1.09E-09
Colorectal cancer	16	2.95E-08
Renal cell carcinoma	16	0.0001941
Gastric acid secretion	16	0.0010539

GnRH signaling pathway	15	3.24E-11
Circadian rhythm	14	3.76E-07
p53 signaling pathway	14	9.83E-07
Lysine degradation	13	3.07E-09
Adherens junction	13	1.57E-06
HTLV-I infection	13	8.50E-06
Endocrine and other factor-regulated calcium reabsorption	13	0.0003858
Protein processing in endoplasmic reticulum	13	0.0111846
Pancreatic cancer	12	1.23E-07
Phosphatidylinositol signaling system	12	0.0010184
Mucin type O-Glycan biosynthesis	12	0.0037809
Calcium signaling pathway	12	0.0051492
Gap junction	11	1.23E-07
Regulation of actin cytoskeleton	11	2.64E-06
Glutamatergic synapse	11	0.0172322
RNA transport	10	1.70E-05
Small cell lung cancer	10	0.0003632
Oocyte meiosis	10	0.0009539
Glycosaminoglycan biosynthesis - chondroitin sulfate	9	3.97E-05
Hedgehog signaling pathway	9	0.0475832
ECM-receptor interaction	8	4.70E-06
Progesterone-mediated oocyte maturation	7	0.0319292
Prion diseases	3	0
Fatty acid biosynthesis	3	2.64E-11

Supplementary Table 6

KEGG pathway	p-value	Targets of miR-424-5p	Targets of let-7d-5p
Insulin signaling pathway	1.64E-07	IRS2,BRAF,FASN,GSK3B,SOS2,RAF1,IKBK B,TRIP10,TSC2,MAPK8,PIK3R1,PRKAR2A,I RS1,INSR,PRKAB2,AKT3,PPARGC1A,PRKA G2,MAP2K1,MKNK1,FOXO1	IRS2,TSC1,NRAS,CALM1,RPS6KB2,M APK8,PRKAR2A
Wnt signaling pathway	5.04E-06	GSK3B,LRP6,WNT7A,BTRC,CCND2,ROCK2, <b>SMAD3</b> ,NFATC4, <b>FZD4</b> ,SENP2,FZD10,AXIN 2,MAPK8,PPP2R1A,SIAH1,WNT3A,NFATC3, PPP2R1B,TBL1XR1,CCND3	PORCN, <b>FZD4</b> ,SENP2,NFAT5,GPC4,M APK8,NKD1,WNT9A
TGF-beta signaling pathway	2.18E-05	SMURF2,ROCK2, <b>SMAD3</b> ,CHRD,PPP2R1A,S MURF1,SMAD5,ACVR2A, <b>SMAD7</b> ,PPP2R1B	<b>TGFBR1</b> , <b>RPS6KB2</b> ,E2F5,ACVR2A,G DF6,ACVR1C
mTOR signaling pathway	4.36E-05	BRAF,IKBKB, <b>TSC2</b> ,EIF4B,PIK3R1,IRS1,RPS 6KA3,AKT3,CAB39,STRADA	TSC1, <b>RPS6KB2</b> ,RICTOR,ULK3,ULK2

The targets with bold were selected as represents of signaling pathways to be detected.

Supplementary Table 7

Figure	Targets	Compared groups	p value
Figure 1C	let-7d-5p	PSP-BHD vs PSP	<b>p=0.0442</b>
	miR-424-5p	PSP-BHD vs PSP	<b>p=0.0089</b>
	miR-199a-3p	PSP-BHD vs PSP	<b>p=0.0493</b>
	miR-194	PSP-BHD vs PSP	p=0.4391
Figure 2A	let-7d-5p	PSP-BHD vs PSP	<b>p&lt;0.0001</b>
		PSP-BHD vs NC	<b>p&lt;0.0001</b>
		PSP vs NC	p=0.4516
	miR-424-5p	PSP-BHD vs PSP	<b>p&lt;0.0001</b>
		PSP-BHD vs NC	<b>p&lt;0.0001</b>
		PSP vs NC	<b>p=0.0056</b>
Figure 3A	FLCN of BEAS-2B cells	siFLCN vs scFLCN	<b>p=0.0029</b>
		Blank vs scFLCN	p=0.1147
	FLCN of HaCaT cells	siFLCN vs scFLCN	<b>p=0.0018</b>
		Blank vs scFLCN	p=0.9795
	FLCN of HEK293 cells	siFLCN vs scFLCN	<b>p=0.0058</b>
		Blank vs scFLCN	p=0.2797
	FLCN of HELF cells	siFLCN vs scFLCN	<b>p=0.0440</b>
		Blank vs scFLCN	p=0.9734
Figure 3B	let-7d-5p of BEAS-2B cells	siFLCN vs scFLCN	<b>p=0.0340</b>
	miR-424-5p of BEAS-2B cells	siFLCN vs scFLCN	<b>p=0.0078</b>
	let-7d-5p of HaCaT cells	siFLCN vs scFLCN	p=0.9548
	miR-424-5p of HaCaT cells	siFLCN vs scFLCN	p=0.0657
	let-7d-5p of HEK293 cells	siFLCN vs scFLCN	p=0.5258
	miR-424-5p of HEK293 cells	siFLCN vs scFLCN	p=0.7201
	let-7d-5p of HELF cells	siFLCN vs scFLCN	p=0.4696
	miR-424-5p of HELF cells	siFLCN vs scFLCN	p=0.7649
Figure 3C	FLCN of A549 cells	wtFLCN vs Vector	<b>p&lt;0.0001</b>

		Blank vs Vector	p=0.7215
		muFLCN vs Vector	p=0.0688
Figure 3D	let-7d-5p of A549 cells	wtFLCN vs Vector	<b>p=0.0134</b>
		Blank vs Vector	p=0.9527
		muFLCN vs Vector	p=0.8036
	miR-424-5p of A549 cells	wtFLCN vs Vector	<b>p=0.0081</b>
		Blank vs Vector	p=0.7730
		muFLCN vs Vector	p=0.6645
Figure 4A	Apoptotic BEAS-2B cells	siFLCN vs scFLCN	<b>p=0.0064</b>
		424 mimic vs mimic NeC	<b>p=0.0017</b>
		siFLCN+424 inhibitor vs siFLCN+inhibitor NeC	<b>p&lt;0.0001</b>
		siFLCN vs siFLCN+inhibitor NeC	p=0.1798
Figure 4B	FLCN	424 mimic vs mimic NeC	p=0.5883
		Blank vs mimic NeC	p=0.4925
	Bim	424 mimic vs mimic NeC	<b>p=0.0056</b>
		Blank vs mimic NeC	p=0.8332
	cl.Cas3	424 mimic vs mimic NeC	<b>p=0.0202</b>
		Blank vs mimic NeC	p=0.9235
Figure 4C	FLCN	siFLCN vs scFLCN	<b>p=0.0039</b>
		Blank vs scFLCN	p=0.4040
	Bim	siFLCN vs scFLCN	<b>p=0.0028</b>
		Blank vs scFLCN	p=0.0694
	cl.Cas3	siFLCN vs scFLCN	<b>p=0.0441</b>
		Blank vs scFLCN	p=0.4584
Figure 4D	FLCN	siFLCN+424 inhibitor vs siFLCN+ inhibitor NeC	p=0.6711
		siFLCN vs siFLCN+ inhibitor NeC	p=0.4740
		Blank vs siFLCN+ inhibitor NeC	<b>p=0.0241</b>
	Bim	siFLCN+424 inhibitor vs siFLCN+ inhibitor NeC	<b>p=0.0031</b>
		siFLCN vs siFLCN+ inhibitor NeC	p=0.9029

		Blank vs siFLCN+ inhibitor NeC	<b>p=0.0273</b>
	cl.Cas3	siFLCN+424 inhibitor vs siFLCN+ inhibitor NeC	<b>p=0.0382</b>
		siFLCN vs siFLCN+ inhibitor NeC	p=0.9369
		Blank vs siFLCN+ inhibitor NeC	<b>p=0.0063</b>
Figure 4E	$\alpha$ -SMA	7d mimic vs mimic NeC	<b>p=0.0239</b>
		424 mimic vs mimic NeC	<b>p=0.0144</b>
		Mimics vs mimic NeC	<b>p=0.0124</b>
		Blank vs mimic NeC	p=0.6757
	Vimentin	7d mimic vs mimic NeC	<b>p=0.0028</b>
		424 mimic vs mimic NeC	<b>p=0.0134</b>
		Mimics vs mimic NeC	<b>p=0.0016</b>
		Blank vs mimic NeC	p=0.8181
	E-Cadherin	7d mimic vs mimic NeC	<b>p=0.0137</b>
		424 mimic vs mimic NeC	<b>p=0.0159</b>
		Mimics vs mimic NeC	<b>p=0.0285</b>
		Blank vs mimic NeC	p=0.4650
	TJP1	7d mimic vs mimic NeC	<b>p=0.0362</b>
		424 mimic vs mimic NeC	<b>p=0.0041</b>
		Mimics vs mimic NeC	<b>p=0.0019</b>
		Blank vs mimic NeC	p=0.7399
Slug	7d mimic vs mimic NeC	<b>p=0.0046</b>	
	424 mimic vs mimic NeC	<b>p=0.0158</b>	
	Mimics vs mimic NeC	<b>p=0.0041</b>	
	Blank vs mimic NeC	p=0.4932	
Figure 5A	FLCN	7d mimic vs mimic NeC	p=0.6228
		424 mimic vs mimic NeC	p=0.9978
		Mimics vs mimic NeC	p=0.5907
		Blank vs mimic NeC	p=0.9204
	Smad7	7d mimic vs mimic NeC	p=0.3752

		424 mimic vs mimic NeC	<b>p=0.0146</b>	
		Mimics vs mimic NeC	<b>p=0.0172</b>	
		Blank vs mimic NeC	p=0.3406	
	Smad3		7d mimic vs mimic NeC	p=0.5579
			424 mimic vs mimic NeC	p=0.6790
			Mimics vs mimic NeC	p=0.7579
	p-Smad3		Blank vs mimic NeC	p=0.9266
			7d mimic vs mimic NeC	p=0.8646
			424 mimic vs mimic NeC	<b>p=0.0008</b>
Figure 5B	FLCN	Mimics vs mimic NeC	<b>p=0.0008</b>	
		Blank vs mimic NeC	p=0.2003	
	Smad7	7d mimic vs mimic NeC	p=0.8646	
		424 mimic vs mimic NeC	<b>p=0.0039</b>	
	Smad3	siFLCN vs scFLCN	<b>p=0.0039</b>	
		Blank vs scFLCN	p=0.3011	
	p-Smad3	siFLCN vs scFLCN	<b>p=0.0019</b>	
		Blank vs scFLCN	p=0.2216	
	Figure 5C	p-Smad3	siFLCN vs scFLCN	p=0.6202
Blank vs scFLCN			p=0.6666	
siFLCN vs scFLCN			<b>p=0.0238</b>	
Bim		Blank vs scFLCN	p=0.5950	
		424 mimic vs DMSO	<b>p=0.0043</b>	
		424 mimic vs mimic+SIS3	<b>p=0.0071</b>	
cl.Cas3		DMSO vs mimic+SIS3	p=0.4066	
		424 mimic vs DMSO	<b>p=0.0015</b>	
		424 mimic vs mimic+SIS3	<b>p=0.0086</b>	
Figure 5D	Smad7	DMSO vs mimic+SIS3	p=0.1464	
		424 mimic vs DMSO	<b>p=0.0168</b>	
		424 mimic vs mimic+SIS3	<b>p=0.0283</b>	
		DMSO vs mimic+SIS3	p=0.7752	
		7d mimic vs mimic NeC	p=0.8269	

		424 mimic vs mimic NeC	p=0.4303	
		Mimics vs mimic NeC	p=0.4179	
		Blank vs mimic NeC	p=0.7524	
	FZD4	7d mimic vs mimic NeC	<b>p=0.0346</b>	
		424 mimic vs mimic NeC	<b>p=0.0178</b>	
		Mimics vs mimic NeC	<b>p=0.0053</b>	
		Blank vs mimic NeC	p=0.5851	
		β-Catenin	7d mimic vs mimic NeC	<b>p=0.0342</b>
			424 mimic vs mimic NeC	<b>p=0.0130</b>
Mimics vs mimic NeC	<b>p=0.0024</b>			
Blank vs mimic NeC	p=0.7963			
Figure 5E	β-Catenin	7d mimic vs mimic+BML	<b>p=0.0137</b>	
		424 mimic vs mimic+BML	<b>p=0.0328</b>	
		7d mimic vs BML	<b>p=0.0004</b>	
		424 mimic vs BML	<b>p=0.0046</b>	
	α-SMA	7d mimic vs mimic+BML	<b>p=0.0345</b>	
		424 mimic vs mimic+BML	<b>p=0.0032</b>	
		7d mimic vs BML	<b>p=0.0233</b>	
		424 mimic vs BML	<b>p=0.0130</b>	
	Slug	7d mimic vs mimic+BML	<b>p=0.0357</b>	
		424 mimic vs mimic+BML	<b>p=0.0125</b>	
		7d mimic vs BML	<b>p=0.0105</b>	
		424 mimic vs BML	<b>p=0.0067</b>	
Figure 5F	Luciferase activity with 424 mimic	muSmad7 vs wtSmad7	<b>p&lt;0.0001</b>	
	Luciferase activity with mimic NeC	muSmad7 vs wtSmad7	p=0.9337	
	Luciferase activity with 7d mimic	muFZD4 vs wtFZD4	<b>p&lt;0.0001</b>	
	Luciferase activity with 424 mimic	muFZD4 vs wtFZD4	<b>p&lt;0.0001</b>	
	Luciferase activity with mimic NeC	muFZD4 vs wtFZD4	p=0.9865	
Figure 6	Growth rate of HELF cells	S vs S+mimic NeC	p=0.0983	

		S +7d mimic vs mimic NeC	<b>p=0.0046</b>
		S +424 mimic vs mimic NeC	<b>p&lt;0.0001</b>
		S + mimics vs mimic NeC	<b>p&lt;0.0001</b>
	Growth rate of BEAS-2B cells	S vs S+mimic NeC	p=0.4209
		S +7d mimic vs mimic NeC	p=0.1393
		S +424 mimic vs mimic NeC	<b>p&lt;0.0001</b>
		S + mimics vs mimic NeC	<b>p=0.0005</b>
Figure 7 C	FLCN	PSP-BHD vs PSP	<b>p=0.0298</b>
		PSP-BHD vs NC	<b>p=0.0104</b>
		PSP vs NC	p=0.5998
	Smad7	PSP-BHD vs PSP	<b>p=0.0016</b>
		PSP-BHD vs NC	<b>p&lt;0.0001</b>
		PSP vs NC	p=0.7811
	p-Smad3	PSP-BHD vs PSP	<b>p=0.0080</b>
		PSP-BHD vs NC	<b>p=0.0141</b>
		PSP vs NC	p=0.4489
	FZD4	PSP-BHD vs PSP	<b>p=0.0026</b>
		PSP-BHD vs NC	<b>p&lt;0.0001</b>
		PSP vs NC	p=0.2301
	β-Catenin	PSP-BHD vs PSP	<b>p=0.0035</b>
		PSP-BHD vs NC	<b>p=0.0003</b>
		PSP vs NC	p=0.4782
	Bim	PSP-BHD vs PSP	<b>p&lt;0.0001</b>
		PSP-BHD vs NC	<b>p=0.0181</b>
		PSP vs NC	p=0.5296
	cl.Cas3	PSP-BHD vs PSP	<b>p=0.0216</b>
		PSP-BHD vs NC	<b>p=0.0048</b>
		PSP vs NC	p=0.3286
	Vimentin	PSP-BHD vs PSP	<b>p=0.0260</b>

		PSP-BHD <i>vs</i> NC	<b>p=0.0062</b>
		PSP <i>vs</i> NC	p=0.4891
	$\alpha$ -SMA	PSP-BHD <i>vs</i> PSP	<b>p=0.0002</b>
		PSP-BHD <i>vs</i> NC	p=0.2455
		PSP <i>vs</i> NC	<b>p=0.0181</b>
	TJP1	PSP-BHD <i>vs</i> PSP	<b>p=0.0498</b>
		PSP-BHD <i>vs</i> NC	p=0.0691
		PSP <i>vs</i> NC	p=0.2465
	Slug	PSP-BHD <i>vs</i> PSP	<b>p=0.0141</b>
		PSP-BHD <i>vs</i> NC	<b>p=0.0076</b>
		PSP <i>vs</i> NC	p=0.8577

## Supplementary figures

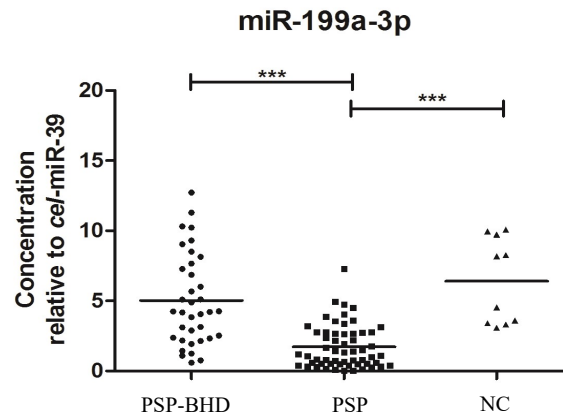


Figure 1. Plasma concentration of miR-199a-3p of PSP-BHD (n=36), PSP (n=57) and normal controls (NC, n=15). The dashes represent the mean values. \*\*\* means  $P < 0.0001$ .

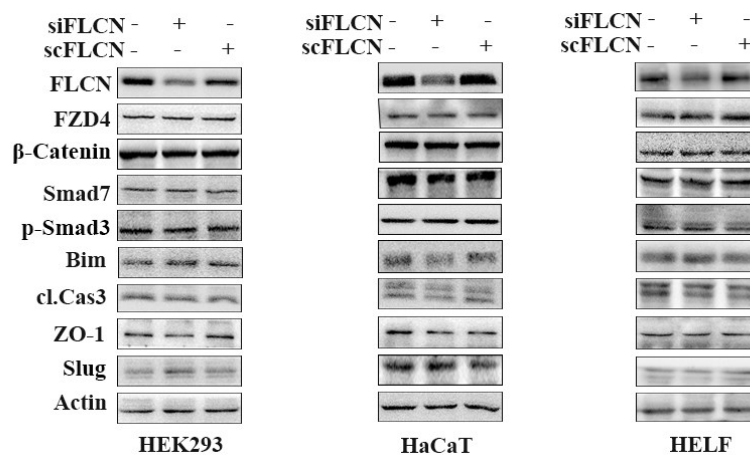


Figure 2. Characteristics of apoptosis and targets observed in BEAS-2B cells with FLCN knockdown were observed in HEK293, HaCaT and HELF cells with FLCN knockdown. siFLCN represents a siRNA of FLCN, scFLCN represents a scramble sequence of FLCN.

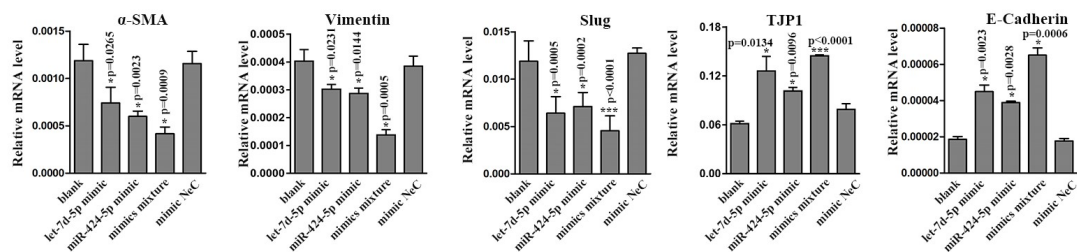


Figure 3. mRNAs of Vimentin,  $\alpha$ -SMA and Slug were reduced significantly while TJP1 and E-Cadherin were increased with miR-424-5p and let-7d-5p mimics. The columns represent mean and the bars indicate standard deviation.

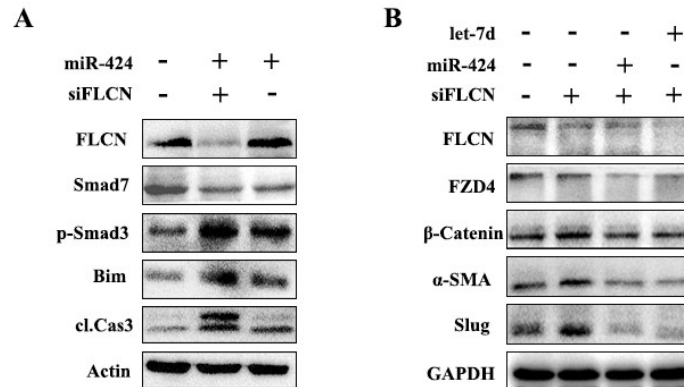


Figure 4. Indicators of apoptosis or MET in BEAS-2B cells or HELF cells with FLCN knockdown and miRNAs mimics. (A) was in BEAS-2B cells and (B) was in HELF cells. miR-424 represents miR-424-5p and let-7d represents let-7d-5p.

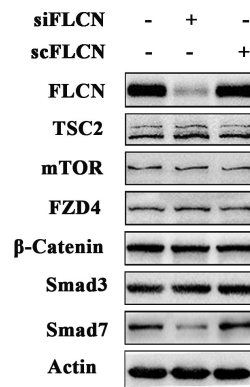


Figure 5. Indicators of WNT, TGF-β and mTOR signaling pathways in condition of FLCN knockdown in BEAS-2B cells. siFLCN means siRNA of FLCN transfection, scFLCN means scramble sequence of FLCN.

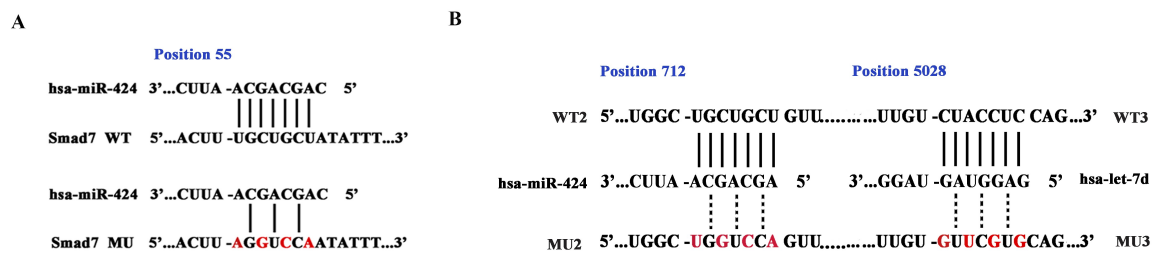
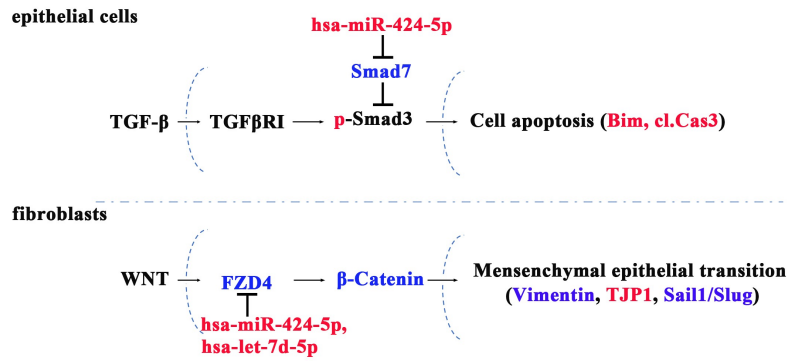
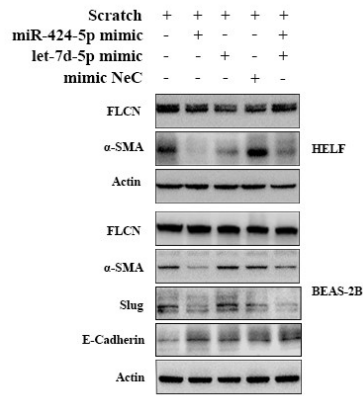


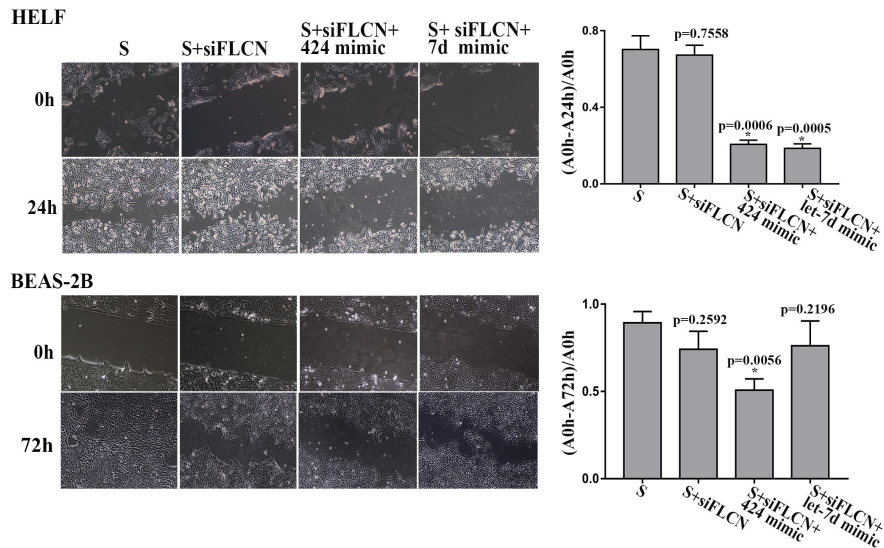
Figure 6. The targeted position of Smad7 by miR-424 (A) and of FZD4 by both miR-424 and let-7d (B) were predicted.



Sfigure 7. A schematic showing evaluated members of TGF-β and WNT pathways in condition of FLCN koncdown/miRNAs mimics.



Sfigure 8. Proteins of woud-healing experiments in HELF and BEAS-2B cells.



Sfigure 9. Cellular wound-healing responses were suppressed by miR-424-5p or let-7d-5p in the condition of FLCN knockdown.

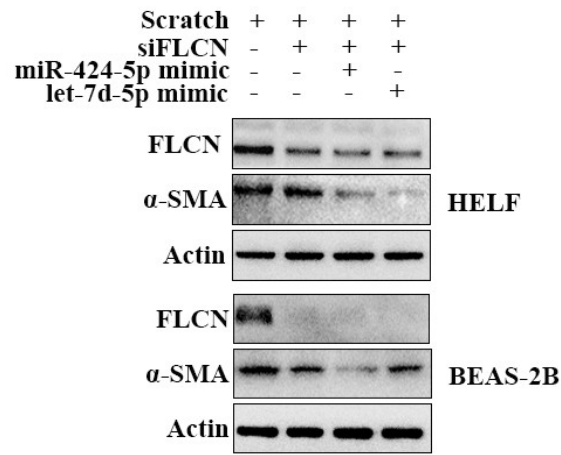


Figure 10. Proteins of wound-healing experiments in HELF and BEAS-2B cells in the condition of FLCN knockdown.